NUMERICAL PREDICTION OF WAVE TRANSMISSION OVER SUBMERGED BREAKWATERS

BY

NOBUHISA KOBAYASHI AND ANDOJO WURJANTO

Sponsored by
U. S. Army Coastal Engineering Research Center

RESEARCH REPORT NO. CE-89-73
MARCH, 1989

CENTER FOR APPLIED COASTAL RESEARCH
DEPARTMENT OF CIVIL ENGINEERING
UNIVERSITY OF DELAWARE
NEWARK, DELAWARE
19716

ABSTRACT

Monochromatic wave reflection and transmission over a submerged impermeable breakwater is predicted numerically by slightly modifying the numerical model developed previously for predicting wave reflection and run-up on rough or smooth impermeable slopes. The slight modification is related to the landward boundary condition required for the transmitted wave propagating landward. In addition to the conservation equations of mass and momentum used to compute the flow field, an equation of energy is derived to estimate the rate of energy dissipation due to wave breaking. The computed reflection and transmission coefficients are shown to be in agreement with available small-scale test data. The numerical model also predicts the spatial variation of the energy dissipation, the mean water level difference, and the time-averaged volume flux per unit width, although available measurements are not sufficient for evaluating the capabilities and limitations of the numerical model for predicting these quantities.

ACKNOWLEDGEMENT

This is the second report resulting from research sponsored by Coastal Engineering Research Center, U.S. Army Engineer Waterways Experiment Station under Contract No. DACW 3988P0628. The authors would like to thank J. P. Ahrens and D. D. Davidson for their enthusiastic support of our efforts to develop a computer program for rubble structure design.

TABLE OF CONTENTS

NUMERICAL PREDICTION OF WAVE TRANSMISSION OVER SUBMERGED BREAKWATERS

PART I: INTRODUCTION

Background

Submerged breakwaters are used for shoreline or harbor protection. Low-crested rubble-mound breakwaters may also become submerged after being damaged or matured (e.g., Adams and Sonu, 1986; Ahrens, 1987). The advantages of submerged breakwaters as compared to subaerial breakwaters include their low cost, aesthetics and effectiveness of triggering breaking of high waves without eliminating the landward flow of water which may be important for water quality considerations as discussed by Diskin et al. (1970) and in the Shore Protection Manual (U.S. Army CERC, 1984), hereafter referred to as SPM.

Most information about wave transmission, reflection and energy dissipation was obtained from hydraulic model tests as summarized in SPM and the report of Seelig (1980). The measurements in the model tests were generally limited to the free surface oscillations on the landward and seaward sides of submerged breakwaters because of ease of instrumentation. These measurements may be sufficient for estimating the wave reflection and transmission coefficients but do not reveal the hydrodynamic processes over submerged breakwaters.

Scope

The numerical model developed by Kobayashi et al. (1987) and Kobayashi and Watson (1987) for predicting the uprush and downrush of normally incident monochromatic waves on rough or smooth impermeable slopes is modified in this report to predict wave transmission over submerged breakwaters. Wave

overtopping over subaerial breakwaters was already examined by Kobayashi and Wurjanto (1988,1989a). The randomness of incident wind waves, the permeability of a rubble-mound breakwater and the stability of armor units are not considered herein. The landward boundary condition for the numerical model is modified assuming that the transmitted waves propagate landward without being reflected from the shoreline and the transmitted water flows landward without a return current. The effects of the shoreline and return current were considered in the analysis of Kobayashi et al. (1989) for the wave transformation over a shore-parallel bar.

In addition to the equations of mass and momentum used for the numerical model, an equation of energy is derived to estimate the spatial variations of energy dissipation rates due to wave breaking and bottom friction. The reflection and transmission coefficients are estimated considering the time-averaged values of the specific energy and energy flux per unit width at the seaward and landward boundaries.

The computed reflection and transmission coefficients are shown to be in agreement with available small-scale data for a submerged impermeable breakwater (Seelig, 1980). The additional quantities computed herein include the difference of the mean water level on the landward and seaward sides of the submerged breakwater as well as the time-averaged volume flux per unit width over the submerged breakwater. These quantities may be of value for predicting a horizontal circulation pattern behind a submerged breakwater.

It should be stated that a concise version of this report will be published elsewhere (Kobayashi and Wurjanto, 1989b and 1989c).

PART II: NUMERICAL MODEL

Governing Equations

The numerical model based on the finite-amplitude shallow-water equations is essentially the same as that used by Kobayashi et al. (1987) except for the landward boundary condition. Fig. 1 shows the two-dimensional coordinate system (x',z') in which the prime indicates the physical variables. The x' coordinate is taken to be positive in the landward direction with $x'=0$ at the seaward toe of a submerged breakwater where the water depth below the still water level (SWL) is given by d_t'. The variation of the local slope angle θ' with respect to x' are used to specify any breakwater geometry in the computation domain $0 \le x \le x_e'$ where x_e' is the x'-coordinate of the landward toe of the submerged breakwater. The water depth below SWL at $x=x_e'$ is denoted by d_e' since d_t' and d_e' may not be the same. The particular geometry of the smooth impermeable submerged breakwater shown in Fig. 1 will be explained when the numerical model is compared with the small-scale data of Seelig (1980).

The equations of conservation of mass and x'-momentum integrated from the assumed impermeable breakwater to the instantaneous free surface located at $z'=\eta'$ may be expressed as

$$\frac{\partial h'}{\partial t'} + \frac{\partial}{\partial x'}\left(h'u'\right) = 0 \tag{1}$$

$$\frac{\partial}{\partial t'}\left(h'u'\right) + \frac{\partial}{\partial x'}\left(h'u'^2 + \frac{1}{2}\,gh'^2\right) = -\,gh'\,\tan\theta' - \frac{1}{2}\,f'|u'|u' \tag{2}$$

in which t' = time; h' = instantaneous water depth; u' = instantaneous depth-averaged horizontal velocity; g = gravitational acceleration; and f' = bottom friction factor. For the subsequent computation for the smooth impermeable breakwater, use is made of $f' = 0.05$ which was found to be satisfactory for

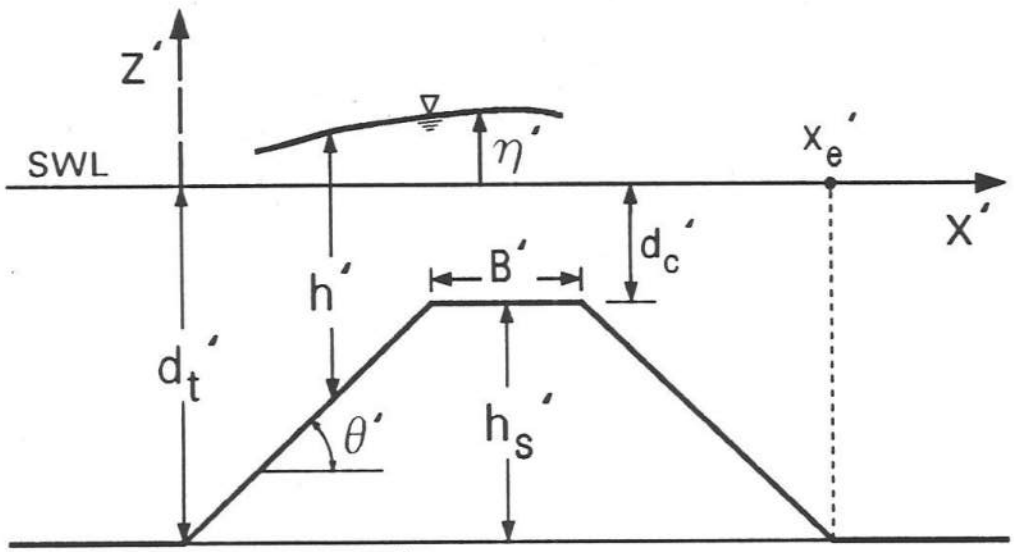

Figure 1. Definition sketch for numerical model and geometry of Breakwater 1 tested by Seelig (1980).

wave run-up and overtopping on small-scale smooth slopes (Kobayashi and Watson, 1987; Kobayashi and Wurjanto, 1988).

For the computation, the following dimensionless variables are introduced:

$$t = \frac{t'}{T'} \quad ; \quad u = \frac{u'}{\sqrt{gH'}} \quad ; \quad x = \frac{x'}{T'\sqrt{gH'}} \quad ; \quad x_e = \frac{x'_e}{T'\sqrt{gH'}} \tag{3}$$

$$z = \frac{z'}{H'} \quad ; \quad h = \frac{h'}{H'} \quad ; \quad \eta = \frac{\eta'}{H'} \quad ; \quad d_t = \frac{d'_t}{H'} \quad ; \quad d_e = \frac{d'_e}{H'} \tag{4}$$

$$\sigma = T'\sqrt{\frac{g}{H'}} \quad ; \quad \theta = \sigma \tan\theta' \quad , \quad f = \frac{1}{2}\sigma f' \tag{5}$$

in which T' = incident monochromatic wave period; H' = incident monochromatic wave height at $x'=0$; σ = dimensionless parameter related to wave steepness; θ = normalized gradient of the local slope; and f = normalized friction factor.

Substitution of Eqs. 3-5 into Eqs. 1 and 2 yields

$$\frac{\partial h}{\partial t} + \frac{\partial}{\partial x}(hu) = 0 \tag{6}$$

$$\frac{\partial}{\partial t}(hu) + \frac{\partial}{\partial x}\left(hu^2 + \frac{1}{2}h^2\right) = -\theta h - f|u|u \tag{7}$$

Eqs. 6 and 7 are solved numerically in the time domain using the explicit dissipative Lax-Wendroff finite difference method based on a finite-difference grid of constant space size and constant time step (Kobayashi et al., 1987). The damping coefficients determining the amount of damping high-frequency numerical oscillations at the rear of breaking wave crests are increased from unity to two because of the discontinuities of θ at the sharp corners of the specific breakwater geometry shown in Fig. 1. The number of spatial grid points in the computation domain $0 \le x \le x_e$ is taken to be 300, while the number of time steps per wave period is taken to be approximately 3,000

considering the numerical stability criterion as well as the desirable spatial and temporal accuracy. The small grid spacing and time step are found to be required for the prediction of time-averaged quantities as will be discussed later.

Initial and Boundary Conditions

The initial time t=0 for the computation marching forward in time is taken to be the time when the specified incident wave train arrives at x=0 and no wave action is present in the computation domain $0 \le x \le x_e$.

In order to derive appropriate seaward and landward boundary conditions, Eqs. 6 and 7 are rewritten in terms of the characteristic variables α and β (Kobayashi et al., 1987)

$$\frac{\partial \alpha}{\partial t} + (u+c)\frac{\partial \alpha}{\partial x} = -\theta - \frac{f|u|u}{h} \quad ; \quad \text{along } \frac{dx}{dt} = u + c \tag{8}$$

$$\frac{\partial \beta}{\partial t} + (u-c)\frac{\partial \beta}{\partial x} = \theta + \frac{f|u|u}{h} \quad ; \quad \text{along } \frac{dx}{dt} = u - c \tag{9}$$

$$\text{with} \quad c = \sqrt{h} \quad ; \quad \alpha = u + 2c \quad ; \quad \beta = -u + 2c \tag{10}$$

The seaward boundary conditions at x=0 are the same as those used by Kobayashi et al. (1987)

$$h = d_t + \eta_i(t) + \eta_r(t) \quad ; \quad \text{at } x = 0 \tag{11}$$

$$\eta_r(t) \simeq \frac{1}{2}\sqrt{d_t}\,\beta(t) - d_t \quad ; \quad \text{at } x = 0 \tag{12}$$

in which η_i and η_r are the free surface oscillations at x=0 normalized by H' due to the incident and reflected waves, respectively. The incident wave train in the water depth d_t is specified by prescribing the periodic variation of η_i with respect to $t \ge 0$. Eq. 12 expresses the reflected wave train η_r in terms of the seaward-advancing characteristics β given by Eq. 9. The value of

u at x=0 is obtained from $u = (2\sqrt{h} - \beta)$ using the computed values of β and h at x=0. Eq. 12 is approximate since use is made of the relationships applicable for linear long waves, $u_i \simeq \eta_i/\sqrt{d_t}$ and $u_r \simeq -\eta_r/\sqrt{d_t}$, where u_i and u_r are the normalized horizontal velocities at x=0 due to the incident and reflected waves, respectively. Previous applications of Eqs. 11 and 12 have suggested that these equations may be satisfactory even when the assumption of linear long waves is not satisfied strictly.

Likewise, the landward boundary conditions at $x = x_e$ may be expressed as

$$h = d_e + \eta_t(t) \quad ; \quad \text{at } x = x_e \tag{13}$$

$$\eta_t \simeq \frac{1}{2}\sqrt{d_e}\,\alpha(t) - d_e \quad ; \quad \text{at } x = x_e \tag{14}$$

where η_t is the normalized free surface oscillation at $x = x_e$ associated with the transmitted wave, provided that no wave propagates seaward from the region $x > x_e$. It is assumed that the flow at $x = x_e$ is subcritical and satisfies the condition $u < c$ at $x = x_e$. Then, α and β represent the characteristics advancing landward and seaward, respectively. Eq. 14 expresses the transmitted wave train η_t in terms of the landward-advancing characteristics, $\alpha = (u + 2\sqrt{h})$, in which use is made of the linear long wave approximations, $2\sqrt{h} \simeq [2\sqrt{d_e} + (\eta_t/\sqrt{d_e})]$ and $u \simeq \eta_t/\sqrt{d_e}$ at $x = x_e$. For the computation, the value of α at $x = x_e$ is obtained from Eq. 8 with $f = 0$ which is approximated by a simple first-order finite difference equation. Eqs. 14 and 13 yield the values of η_t and h at $x = x_e$, respectively, while the value of u at $x = x_e$ is obtained from $u = (\alpha - 2\sqrt{h})$ at $x = x_e$.

Reflected and Transmitted Wave Trains

For the incident monochromatic wave train $\eta_i(t)$, the computed temporal variations of $\eta_r(t)$ and $\eta_t(t)$ for $t \geq t_p$ are found to consist of oscillatory and steady components where t_p = normalized time when the periodicity of the oscillatory components is established and the steady components become independent of t.

The reflection coefficient r_1 may be estimated as the normalized height of the oscillatory component of $\eta_r(t)$, whereas the transmission coefficient T_1 may be taken as that of $\eta_t(t)$ if $d_e = d_t$

$$r_1 = (\eta_r)_{max} - (\eta_r)_{min} \quad ; \quad \text{during } t_p \leq t \leq (t_p + 1) \tag{15}$$

$$T_1 = (\eta_t)_{max} - (\eta_t)_{min} \quad ; \quad \text{during } t_p \leq t \leq (t_p + 1) \tag{16}$$

in which the subscripts max and min indicate the maximum and minimum values during one wave period $t_p \leq t \leq (t_p + 1)$. For the computation made in this paper, $t_p = 4$ is found to be sufficient for the periodicity as will be shown later. Kobayashi et al. (1987,1989) used Eq. 15 to predict the reflection coefficient. However, the reflection and transmission coefficients can also be estimated considering the wave energy balance which will be examined in Part III.

On the other hand, the steady components of $\eta_r(t)$ and $\eta_t(t)$ are denoted by $\overline{\eta_r}$ and $\overline{\eta_t}$ in which the overbar indicates the time averaging during $t_p \leq t \leq (t_p + 1)$. Since $\eta = (\eta_i + \eta_r)$ at x=0 and $\eta = \eta_t$ at $x=x_e$, the increase of the normalized mean water level $\bar{\eta}$ from x=0 to $x=x_e$ is given by

$$\Delta\bar{\eta} = \overline{\eta_t} - (\overline{\eta_i} + \overline{\eta_r}) = \overline{\eta_t} - \overline{\eta_r} \tag{17}$$

in which the incident monochromatic wave train $\eta_i(t)$ is specified such that $\overline{\eta_i} = 0$ in this report. It may be noted that the present numerical model is based on the instantaneous mass and momentum equations given by Eqs. 1 and 2 which also yield the time-averaged quantities such as $\bar{\eta}$ and $\bar{u}$ (Kobayashi et al., 1989).

To check the accuracy of the computation, use is made of the time-averaged mass equation corresponding to Eq. 6 which can be rewritten as

$$\bar{m} = \overline{hu} = \text{constant} \tag{18}$$

in which $m = hu$ is the volume flux per unit width. The landward boundary conditions given by Eqs. 13 and 14 are essentially based on the assumption of open water in the region $x > x_e$. The constant volume flux $\bar{m}$ is expected to be positive since the transmission of wave energy will accompany the transmission of water mass over the submerged breakwater.

PART III: WAVE ENERGY BALANCE

Hydraulic test results for wave reflection and transmission over breakwaters are normally analyzed considering the wave energy balance (e.g., Seelig, 1980; Ahrens, 1987), whereas the present numerical model is based on the instantaneous mass and momentum equations expressed by Eqs. 1 and 2. For steady flow in a frictionless horizontal channel with $f'=0$ and $\tan\theta'=0$, Eqs. 1 and 2 reduce to the mass and momentum equations used for the analysis of a hydraulic jump in open channel flow (e.g., Henderson, 1966). Invoking the analogy between wave breaking and hydraulic jumping, an equation of energy may be used to estimate the rate of energy dissipation due to wave breaking without analyzing the dissipation processes explicitly.

Instantaneous Energy Equation

The equation of energy corresponding to Eqs. 1 and 2 may be expressed as

$$\frac{\partial E'}{\partial t'} + \frac{\partial}{\partial x'}\left(E_F'\right) = -D_f' - D_B' \tag{19}$$

with

$$E' = \frac{\rho}{2}\left(h'u'^2 + g\eta'^2\right) \tag{20}$$

$$E_F' = \rho g h' u' \left(\frac{u'^2}{2g} + \eta'\right) \tag{21}$$

$$D_f' = \frac{\rho}{2} f' |u'| u'^2 \tag{22}$$

in which ρ = fluid density; E' = specific energy defined as the sum of kinetic and potential energy per unit horizontal area; E_F' = energy flux per unit width; D_f' = rate of energy dissipation per unit horizontal area due to bottom friction; and D_B' = rate of energy dissipation per unit horizontal area due to wave breaking. Eq. 19 may be used to estimate D_B' invoking the analogy between the present analysis and that used for a hydraulic jump. However, it should

be mentioned that the temporal and spatial variations of D_B' obtained from Eq. 19 may not be very accurate since the present numerical model does not predict the details of wave breaking nor account for the dissipation processes explicitly (Kobayashi et al., 1987 and 1989).

Using Eqs. 3-5, Eqs. 19-22 are expressed in terms of the dimensionless variables

$$\frac{\partial E}{\partial t} + \frac{\partial}{\partial x}(E_F) = - D_f - D_B \tag{23}$$

$$\text{with } E = \frac{E'}{\rho g H'^2} = \frac{1}{2}(hu^2 + \eta^2) \tag{24}$$

$$E_F = \frac{E_F'}{\rho g H'^2 \sqrt{gH'}} = hu\left(\frac{1}{2}u^2 + \eta\right) \tag{25}$$

$$D_f = \frac{T' D_f'}{\rho g H'^2} = f|u|u^2 \tag{26}$$

$$D_B = \frac{T' D_B'}{\rho g H'^2} \tag{27}$$

Time-Averaged Energy Equation

The wave energy balance is normally analyzed in terms of the time-averaged quantities. The spatial variations of $\overline{E}$, $\overline{E_F}$ and $\overline{D_f}$ in the region $0 \le x \le x_e$ are computed using Eqs. 24, 25 and 26, respectively. The time-averaged dissipation rate, $\overline{D_B}$, due to wave breaking is computed using the following time-averaged energy equation obtained from Eq. 23.

$$\frac{d}{dx}\left(\overline{E_F}\right) = - \overline{D_f} - \overline{D_B} \tag{28}$$

Eq. 28 implies that the time-averaged energy flux $\overline{E_F}$ decreases in the landward direction where $\overline{D_f} > 0$ because of Eq. 26 and $\overline{D_B}$ is expected to be positive or zero. Integration of Eq. 28 with respect to x yields the time-averaged energy equation for the region $0 \le x \le x_e$

$$\overline{E_F}(x=0) - \overline{E_F}(x=x_e) = \int_0^{x_e} (\overline{D_f} + \overline{D_B})dx \tag{29}$$

in which the first and second terms on the left hand side of Eq. 29 are the values of $\overline{E_F}$ at $x=0$ and $x=x_e$, respectively.

Linear Wave Approximations at Boundaries

The hydrodynamic problem considered herein is nonlinear especially in the region of wave breaking. Nevertheless, the locations of $x=0$ and $x=x_e$ may be chosen so that nonlinear effects are sufficiently small in the vicinity of $x=0$ and $x=x_e$. This is also the case with laboratory experiments where linear wave theory is normally used to separate the incident and reflected waves in front of a coastal structure (e.g., Goda and Suzuki, 1976; Seelig, 1980).

Using the linear long wave approximations employed to derive Eqs. 12 and 14 together with Eqs. 11 and 13, the time-averaged values of E and E_F given by Eqs. 24 and 25 may be approximated by

$$\overline{E} \simeq \overline{\eta_i^2} + \overline{\eta_r^2} \quad ; \quad \text{at } x = 0 \tag{30}$$

$$\overline{E_F} \simeq \sqrt{d_t}\ (\overline{\eta_i^2} - \overline{\eta_r^2}) \quad ; \quad \text{at } x = 0 \tag{31}$$

$$\overline{E} \simeq \overline{\eta_t^2} \quad ; \quad \text{at } x = x_e \tag{32}$$

$$\overline{E_F} \simeq \sqrt{d_e}\ \overline{\eta_t^2} \quad ; \quad \text{at } x = x_e \tag{33}$$

in which $\sqrt{d_t}$ and $\sqrt{d_e}$ are the normalized group velocities based on linear long wave theory at $x=0$ and $x=x_e$, respectively. $\sqrt{d_t}$ and $\sqrt{d_e}$ may be replaced by the corresponding normalized group velocities in finite water depth if the long wave assumption is not satisfied strictly.

In Eqs. 30-33, $\overline{\eta_i^2}$, $\overline{\eta_r^2}$ and $\overline{\eta_t^2}$ are the normalized wave energy per unit horizontal area associated with the incident, reflected and transmitted waves, respectively, and are the same for linear long wave theory and linear wave theory in finite water depth. Substitution of Eqs. 31 and 33 into Eq. 29 yields the time-averaged energy equation based on linear wave theory which is generally used to estimate the time-averaged rate of energy dissipation caused by the combined effects of bottom friction and wave breaking.

Reflection and Transmission Coefficients

The reflection coefficient r_2 based on the normalized reflected wave energy may be estimated as

$$r_2 = \left[\overline{\eta_r^2} \quad (\overline{\eta_i^2})^{-1} \right]^{1/2} \tag{34}$$

For the case of $d_e = d_t$, the transmission coefficient T_2 based on the normalized transmitted wave energy may be estimated as

$$T_2 = \left[\overline{\eta_t^2} \quad (\overline{\eta_i^2})^{-1} \right]^{1/2} \tag{35}$$

For the sinusoidal variation of $\eta_i(t)$ whose height and period are unity, $\overline{\eta_i^2} = (1/8)$. If the temporal variations of $\eta_r(t)$ and $\eta_i(t)$ are sinusoidal, $\overline{\eta_r^2} = (r_1^2/8)$ and $\overline{\eta_t^2} = (T_1^2/8)$ in which r_1 and T_1 are the normalized heights of η_r and η_t as defined in Eqs. 15 and 16, respectively. Then, Eqs. 34 and 35 yield $r_2 = r_1$ and $T_2 = T_1$, respectively.

Eqs. 34 and 35 do not account for the difference between the still water level and the mean water level. Since $\bar{\eta} = \overline{\eta_r}$ and $\overline{\eta_i} = 0$ at $x=0$ and $\bar{\eta} = \overline{\eta_t}$ at $x=x_e$ as explained in relation to Eq. 17, the reflection coefficient r_3 and the transmission coefficient T_3 accounting for the wave-induced mean water level may be expressed as

$$r_3 = \left[\overline{(\eta_r - \overline{\eta_r})^2}\ (\overline{\eta_i^2})^{-1}\right]^{1/2} = \left[r_2^2 - (\overline{\eta_r})^2\ (\overline{\eta_i^2})^{-1}\right]^{1/2} \tag{36}$$

$$T_3 = \left[\overline{(\eta_t - \overline{\eta_t})^2}\ (\overline{\eta_i^2})^{-1}\right]^{1/2} = \left[T_2^2 - (\overline{\eta_t})^2\ (\overline{\eta_i^2})^{-1}\right]^{1/2} \tag{37}$$

Eqs. 36 and 37 imply that $r_3 < r_2$ and $T_3 < T_2$ as long as $\overline{\eta_r}$ and $\overline{\eta_t}$ are not zero.

Comparison will be made later of the reflection coefficients r_1, r_2 and r_3 given by Eqs. 15, 34 and 36, respectively, and the transmission coefficients T_1, T_2 and T_3 given by Eqs. 16, 35 and 37, respectively. The method used to compute the reflection and transmission coefficients should be consistent with the method used to determine the refection and transmission coefficients from the measured free surface oscillations in experiments. The reflection and transmission coefficients obtained in the model tests of Seelig (1980) essentially correspond to r_3 and T_3 as will be explained in the following.

PART IV: COMPARISON WITH AVAILABLE DATA

Data Used for Comparison

Seelig (1980) conducted extensive small-scale tests on monochromatic and random wave reflection and transmission over and through breakwaters. Only a part of a wide tank was used to minimize the effects of wave reflection from the piston-type wavemaker. Transmitted waves were absorbed at the end of the tank and water overtopping the test structure was allowed to escape through the adjacent gravel absorber beach. As a result, the landward boundary conditions expressed by Eqs. 13 and 14 may be appropriate for these tests.

The numerical model is compared with the test runs for Breakwater 1 which was a smooth impermeable structure located on the horizontal floor as shown in Fig. 1. The height and crest width of the structure were given by h'_s = 75 cm and B' = 30 cm, respectively. The local slope was specified as $\tan\theta' = (2/3)$ for $0 < x' < 1.5\ h'_s$, $\tan\theta' = 0$ for $1.5\ h'_s < x' < (1.5\ h'_s + B')$, and $\tan\theta' = (-2/3)$ for $(1.5\ h'_s + B') < x' < (3\ h'_s + B')$. The landward toe of the breakwater was located at $x' = x'_e$ = 255 cm.

The test runs considered herein are limited to monochromatic waves over Breakwater 1 whose crest was at or below the still water level (SWL). For these tests, $d'_t = d'_e$ = 75, 80, 85 and 90 cm and hence d'_c = 0, 5, 10 and 15 cm where d'_c = water depth below SWL on the crest of the submerged breakwater. Among these tests, fourteen test runs with $d'_t/(gT'^2) = 0.016$ and $d'_c < 3H'$ are selected for the subsequent computation and comparison where T' = monochromatic wave period; and H' = incident wave height in front of the structure. The measured reflection coefficients were plotted for the tests with $d'_t/(gT'^2) = 0.016$, although the measured transmission coefficients were

tabulated for all the tests. The test results with $d_c' < 3H'$ may be regarded to be of practical interest. For the selected fourteen test runs, $T' = 2.18 - 2.39$ s and $H' = 0.6 - 19$ cm.

The numerical model is compared with the fourteen test runs summarized in Table 1. The dimensionless parameters $x_e = [x_e'/(T'\sqrt{gH'})]$, $d_t = (d_t'/H')$ and $\sigma = (T'\sqrt{g/H'})$ have been introduced in Eqs. 3, 4 and 5, respectively. The dimensionless parameters d_c, L and U_r in Table 1 are defined as $d_c = (d_c'/H')$, $L = (L'/d_t')$ and $U_r = (L^2/d_t)$ in which d_c = normalized water depth below SWL on the crest of the submerged breakwater; L = normalized wavelength at x=0; L' = wavelength at x=0 based on linear wave theory; and U_r = Ursell parameter at x=0 (e.g., Dean and Dalrymple, 1984).

For the tests shown in Table 1, $0 \le d_c \le 2.63$ and $0.71 \le x_e \le 4.82$. For the runs with $d_c = 0$, use is made of $d_c = 10^{-3}$ for the computation so that the 300 grid points in the region $0 \le x \le x_e$ used for the computation are located below SWL. For the runs with relatively large values of d_c, wave breaking may not occur over the crest of the submerged breakwater but the present numerical model is applicable to non-breaking waves as long as the horizontal length of the computation domain is not too large relative to the wavelength (Kobayashi et al., 1989). For these tests, the width of the breakwater is on the order of the wavelength which varies in the region $0 \le x \le x_e$.

The surf similarity parameter ξ defined as $\xi = (\sigma \tan\theta'/\sqrt{2\pi})$ (e.g., Kobayashi et al., 1987) varies in the region $0 \le x \le x_e$ and may not be an important parameter for submerged breakwaters. Using $\tan\theta' = (2/3)$, $3.9 \le \xi \le 23.4$ corresponding to surging waves on a 1:1.5 smooth slope in the absence of wave overtopping.

TABLE 1. - Fourteen Test Runs Compared with Numerical Model

Run No.	d_c' (cm)	d_c	x_e	d_t	σ	L	U_r
1	15	1.56	1.10	9.4	24.2	7.05	5.3
2	15	0.78	0.78	4.7	17.0	7.05	10.7
3	10	1.85	1.51	15.7	31.3	7.04	3.2
4	10	0.88	1.04	7.5	21.6	7.04	6.6
5	10	0.41	0.71	3.5	14.7	7.04	14.3
6	5	2.63	2.63	42.1	51.1	7.04	1.2
7	5	1.32	1.86	21.1	36.2	7.04	2.4
8	5	0.64	1.30	10.3	25.2	7.04	4.8
9	5	0.31	0.90	4.9	17.5	7.04	10.0
10	0	0.00	4.82	125.	88.1	7.05	0.4
11	0	0.00	3.56	68.2	65.1	7.05	0.7
12	0	0.00	2.46	32.6	45.0	7.05	1.5
13	0	0.00	1.72	16.0	31.5	7.05	3.1
14	0	0.00	1.19	7.7	21.8	7.05	6.5

For the fourteen runs, $d_t = d_e \geq 3.5$ and $U_r \leq 14.3$, so that nonlinear effects may be sufficiently small in the vicinity of the landward and seaward boundaries. Since L = 7.04 or 7.05, the assumption of long wave is not strictly satisfied in the vicinity of the landward and seaward boundaries. This problem is related to the fact that there is no general wave theory applicable from deep water to shallow water where wave breaking occurs.

For each of the fourteen runs, the normalized incident wave profile $\eta_i(t)$ with unit wave height and period for $t \geq 0$ is estimated using Stokes second-order wave theory which yields the same wavelength as linear wave theory (e.g., Dean and Dalrymple, 1984)

$$\eta_i(t) = a_1 \cos[2\pi(t+t_0)] + a_2 \cos[4\pi(t+t_0)] \quad ; \quad \text{for } t \geq 0 \tag{38}$$

where $a_1 = 0.5$; t_0= time shift introduced to make $\eta_i = 0$ at t=0; and a_2 = normalized amplitude of the second-order harmonic which depends on the values of d_t and L listed in Table 1. For the fourteen runs, $0.003 \leq a_2 \leq 0.111$.

It should be mentioned that Seelig (1980) used the method of Goda and Suzuki (1976) based on linear wave theory to estimate the incident and reflected waves from the free surface oscillations measured at three locations in front of the structure. The mean water level and linear trend were removed from the measured free surface oscillations. As a result, the present computation performed in the time domain does not reproduce the experimental results exactly. Nevertheless, Seelig (1980) indicated that for the selected runs with $d_t'/(gT'^2) = 0.016$, approximately 95 percent of the incident wave energy was at the period of the sinusoidal motion of the wave generator. For the selected fourteen runs, $(a_2/a_1)^2 \leq 0.049$ and Eq. 38 may be regarded as a good approximation.

Discussion on Computed Results

The computed results for the fourteen runs summarized in Table 1 are presented in Appendix B. The computed results for Run No. 8 are discussed in detail as a typical run among these runs.

Fig. 2 shows the specified incident wave train $\eta_i(t)$ with $a_2 = 0.037$ and the computed reflected wave train $\eta_r(t)$ at x=0 as well as the computed transmitted wave train $\eta_t(t)$ at $x = x_e$ for Run No. 8. The temporal variations of η_r and η_t become periodic before $t = t_p = 4$. The computed variations of $\eta_r(t)$ and $\eta_t(t)$ during $4 \leq t \leq 5$ are used to compute the reflection coefficients r_1, r_2 and r_3 defined by Eqs. 15, 34 and 36, respectively, and the transmission coefficients T_1, T_2 and T_3 defined by Eqs. 16, 35 and 37, respectively. Use is made of $\overline{\eta_i^2} = (1/8)$ in Eqs. 34-37 to be consistent with the data analysis based on linear wave theory performed by Seelig (1980). The difference between the mean and still water levels is given by $\overline{\eta_r}$ at x=0 and $\overline{\eta_t}$ at $x=x_e$ which are needed in Eqs. 36 and 37, respectively. The numerical model predicts the wave set-down $\overline{\eta_r} = -0.087$ at x=0 and the wave setup $\overline{\eta_t} = 0.087$ at $x=x_e$. It should be noted that $\overline{\eta_i}$ is computed to be 5×10^{-5} and almost exactly zero.

The computed reflection coefficients are $r_1 = 0.55$, $r_2 = 0.55$ and $r_3 = 0.50$, while the measured reflection coefficient denoted by r_m was $r_m = 0.42$. The computed transmission coefficients are $T_1 = 0.71$, $T_2 = 0.67$ and $T_3 = 0.62$, while the measured transmission coefficient denoted by T_m was $T_m = 0.61$. Considering the data analysis procedure adopted by Seelig (1980), the coefficients r_3 and T_3, which are based on the wave energy and account for the effect of the mean water level, may be regarded to correspond to r_m and T_m, respectively. The agreement between the measured and computed coefficients is

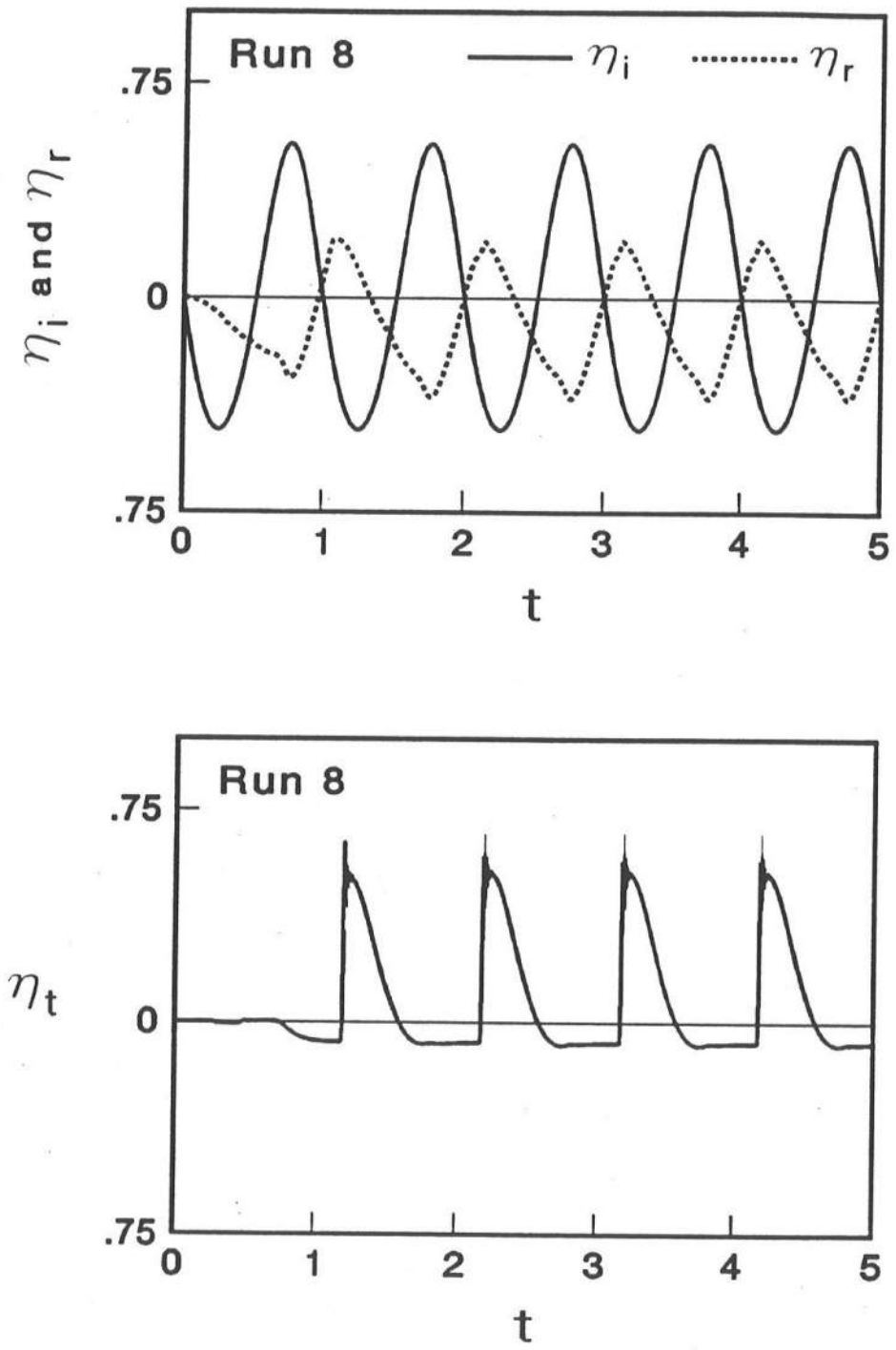

Figure 2. Specified incident wave train $\eta_i(t)$ and computed reflected wave train $\eta_r(t)$ at x=0 as well as computed transmitted wave train $\eta_t(t)$ at $x=x_e$ for Run No. 8.

fairly good although the comparison does not indicate whether the computed wave profiles $\eta_r(t)$ and $\eta_t(t)$ shown in Fig. 2 are correct.

The asymmetry of the profile $\eta_r(t)$ was also noticed in the computed profiles for the case of wave overtopping over a subaerial breakwater (Kobayashi and Wurjanto, 1988), but more symmetric profiles were predicted for the case of no wave overtopping (Kobayashi et al., 1987).

On the other hand, the computed profile $\eta_t(t)$ shown in Fig. 2 exhibits a bore-like profile even though the normalized water depth below SWL is d_e = 10.3 at $x=x_e$. The bore-like profile at $x = x_e = 1.30$ may still be realistic considering the short horizontal distance from the point of wave breaking to the landward boundary located at $x = x_e$. The transmitted bore-like wave may eventually become undular as it propagates further landward. The development of an undular bore was predicted numerically by Peregrine (1966) using the Boussinesq equations based on the assumption of irrotational flow. In any case, data on the wave transformation behind the submerged breakwater will be required to clarify the limitation and capability of the present numerical model.

Fig. 3 shows the computed spatial variations of the normalized free surface elevation η above SWL located at z=0 and the normalized depth-averaged horizontal velocity u at t=4, 4.25, 4.5, 4.75 and 5 for Run No. 8. The spatial variations of η and u at t=4 and 5 are identical because of the periodicity of the computed flow field. Fig. 3 indicates the complicated free surface and velocity variations due to wave breaking in the vicinity of the crest of the submerged breakwater which is depicted in the solid line in the region $-4 \le z \le -d_c$ with $d_c = 0.64$.

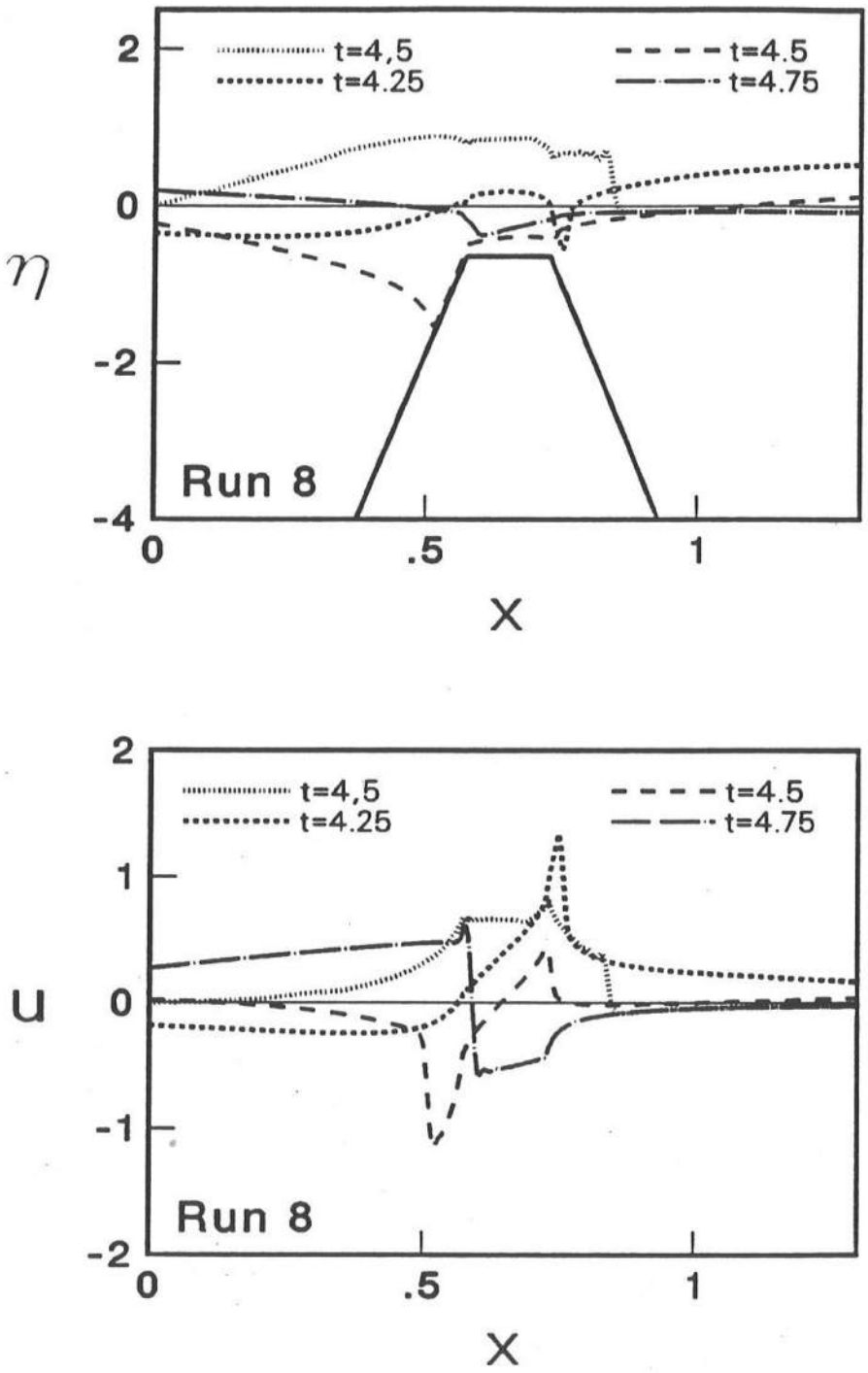

Figure 3. Computed spatial variations of free surface elevation η and horizontal velocity u at t = 4, 4.25, 4.5, 4.75 and 5 for Run No. 8.

It should be stated that the present numerical model is not expected to predict the details of wave breaking and flow separation may occur at the sharp corners of the breakwater. The computed variations of $\eta(t,x)$, $h(t,x)$ and $u(t,x)$ in the region $0 \leq x \leq x_e$ during $4 \leq t \leq 5$ are used to examine the time-averaged wave energy balance in which h is the sum of η and the normalized water depth below SWL.

The time-averaged volume flux per unit width, $\bar{m} = \overline{uh}$, is also computed as a function of x to check whether Eq. 18 is satisfied. For Run No. 8, $\bar{m} = 0.30$ except that the variation of $\bar{m}$ with respect to x exhibits some numerical oscillations and spikes in the vicinity of the sharp corners of the breakwater. As a result, the value of $\bar{m}$ for each run presented in this report is the value at $x = x_e$ representing the constant value of $\bar{m}$.

Fig. 4 shows the computed spatial variations of the time-averaged energy flux per unit width, $\overline{E_F}$, the time-averaged wave energy per unit horizontal area, $\bar{E}$, the time-averaged rate of energy dissipation per unit horizontal area due to bottom friction, $\overline{D_f}$, and the time-averaged rate of energy dissipation per unit horizontal area due to wave breaking, $\overline{D_B}$, for Run No. 8. Eq. 28 is used to estimate $\overline{D_B}$ using the computed spatial variations of $\overline{E_F}$ and $\overline{D_f}$. However, the computed variation of $\overline{E_F}$ is found to exhibit kinks because of the discontinuities of θ in Eq. 7 at the sharp corners and is smoothed so that $\overline{E_F}$ decreases monotonically with respect to x and $\overline{D_B}$ is positive or zero. The smoothing of the computed values of $\overline{E_F}$ at 300 grid points is performed by averaging the computed values of $\overline{E_F}$ at five adjacent grid points and applying the five-point smoothing procedure of Longuet-Higgins and Cokelet (1976) to the averaged values of $\overline{E_F}$ at 60 grid points.

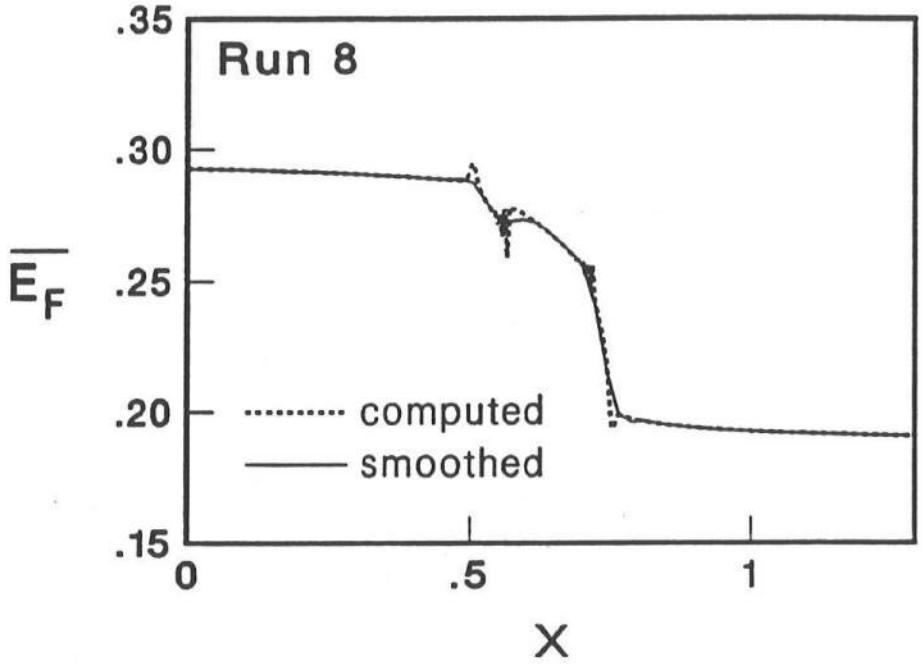

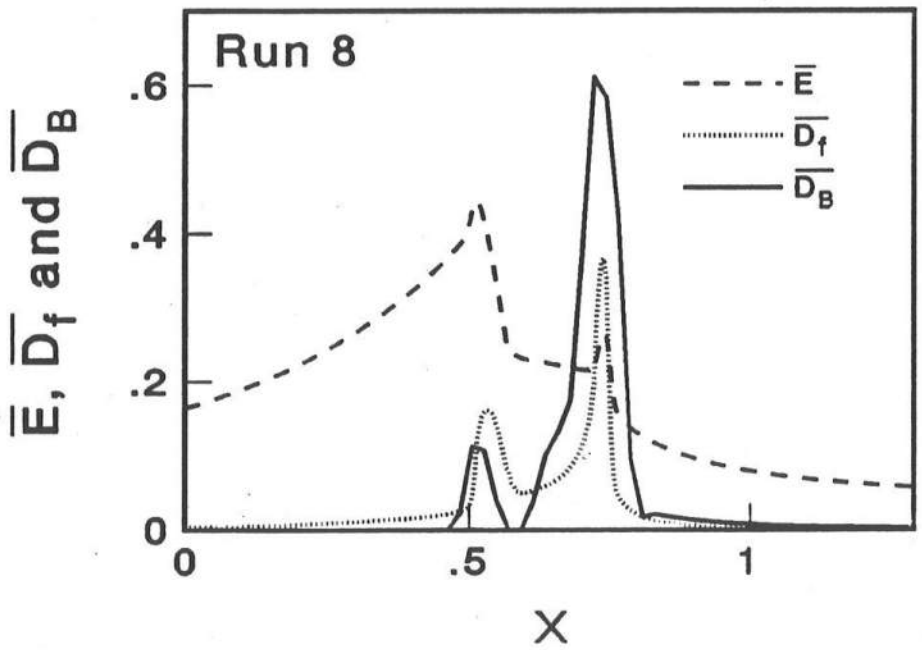

Figure 4. Computed spatial variations of energy flux $\overline{E_F}$, specific energy $\overline{E}$, dissipation rate $\overline{D_f}$ and $\overline{D_B}$ due to bottom friction and wave breaking, respectively, for Run No. 8.

The computed and smoothed variations of $\overline{E_F}$ shown in Fig. 4 are almost indistinguishable apart from the kinks. Moreover, the estimated spatial variation of $\overline{D_B}$ almost satisfies the time-averaged energy equation in the region $0 \leq x \leq x_e$ given by Eq. 29 in which $\overline{E_F}$ $(x=0) = 0.293$ and $\overline{E_F}$ $(x=x_e) = 0.191$, whereas the integration of $(\overline{D_f} + \overline{D_B})$ in the region $0 \leq x \leq x_e$ yields 0.104.

Fig. 4 suggests that the wave energy dissipation due to wave breaking and bottom friction is large in the vicinity of the landward corner of the crest of the breakwater where wave breaking appears to occur as shown in Fig. 3. This statement is intended to be only qualitative because of the smoothing of $\overline{E_F}$ as well as the assumed constant friction factor $f' = 0.05$ without regard to possible flow separation.

The computed spatial variation of $\overline{E}$ shows the increase of $\overline{E}$ due to shoaling on the seaward slope of the breakwater and the decrease of $\overline{E}$ on the crest and the landward slope of the breakwater. For Run No. 8 with $d_c = 0.64$ shown in Fig. 4, the maximum value of $\overline{E}$ occurs seaward of the location of the maximum values of $\overline{D_B}$ and $\overline{D_f}$. Data on the flow field over the crest of the breakwater would be required to examine the detailed processes of wave breaking and evaluate the quantitative accuracy of the predicted wave energy balance such as that shown in Fig. 4.

The approximate relationships given by Eqs. 30-33 are examined to quantify the uncertainties associated with the linear long wave approximations used at $x=0$ and $x=x_e$. The computed values of $\overline{E}$ and $\overline{E_F}$ at $x=0$ are 0.164 and 0.293, respectively, as compared to 0.163 and 0.278 on the right hand sides of Eqs. 30 and 31, respectively. On the other hand, Eqs. 32 and 33 yield $\overline{E} = 0.057 \simeq \overline{\eta_t^2} = 0.055$ and $\overline{E_F} = 0.191 \simeq \sqrt{d_e}\ \overline{\eta_t^2} = 0.178$ at $x=x_e$, respectively. As

a result, Eqs. 33-33 are good approximations for Run No. 8.

The computed results for Run No. 2 are shown in Figs. 5, 6 and 7 which correspond to Figs. 2, 3 and 4 for Run No. 8, respectively. Comparison of these figures may confirm that the computed results for Run No. 8 discussed in detail are fairly typical of the fourteen runs listed in Table 1. However, for Run No. 2 with $d_c = 0.78$, the maximum values of $\overline{E}$, $\overline{D_B}$ and $\overline{D_f}$ shown in Fig. 7 occur approximately at the same location unlike those shown in Fig. 4 for Run No. 8.

Measured and Computed Transmission Coefficients

For each of the fourteen runs listed in Table 1, the computed transmission coefficients T_1, T_2 and T_3 are compared with the measured transmission coefficient T_m as shown in Fig. 8. The solid line in Fig. 8 corresponds to the perfect agreement. T_2 and T_3 given by Eqs. 35 and 37, respectively, are based on the transmitted wave energy and in agreement with T_m based on the measured transmitted wave energy. The effect of the wave-induced mean water level $\overline{\eta_t}$ included in T_3 is minor and does not improve the overall agreement significantly. T_1 given by Eq. 16 is based on the normalized height of the transmitted wave and tends to be greater than T_m since the computed transmitted wave profile $\eta_t(t)$ tends to exhibit a sharp peak as shown in Figs. 2 and 5.

Seelig (1980) proposed the following formula for the empirical wave transmission coefficient, T_e, which is also included in SPM

$$T_e = \left(0.51 - 0.11 \frac{B'}{h_s'}\right) \left(1 + \frac{d_c'}{R'}\right) \tag{39}$$

in which R' = wave run-up on the seaward slope of a breakwater in the absence of wave transmission. For the submerged breakwater under consideration, B' = 30 cm, h_s' = 75 cm and d_c' = 0 - 15 cm as given in Table 1. Eq. 39 was proposed for subaerial breakwaters with $d_c' < 0$ as well. For each of the fourteen runs in Table 1, the value of R' has been estimated using the empirical formula given in the report of Seelig (1980) as well as that given in SPM. The latter has found to yield slightly better agreement between T_e and T_m and is adopted herein. The comparison between T_e and T_m for each of the fourteen runs is shown in Fig. 9 where the computed transmission coefficient T_3 is also plotted for each run to compare the capabilities of the numerical model and the empirical formula given by Eq. 39. For the case of $d_c' = 0$, Eq. 39 yields T_e = 0.47 independent of the incident wave conditions and does not represent the data well.

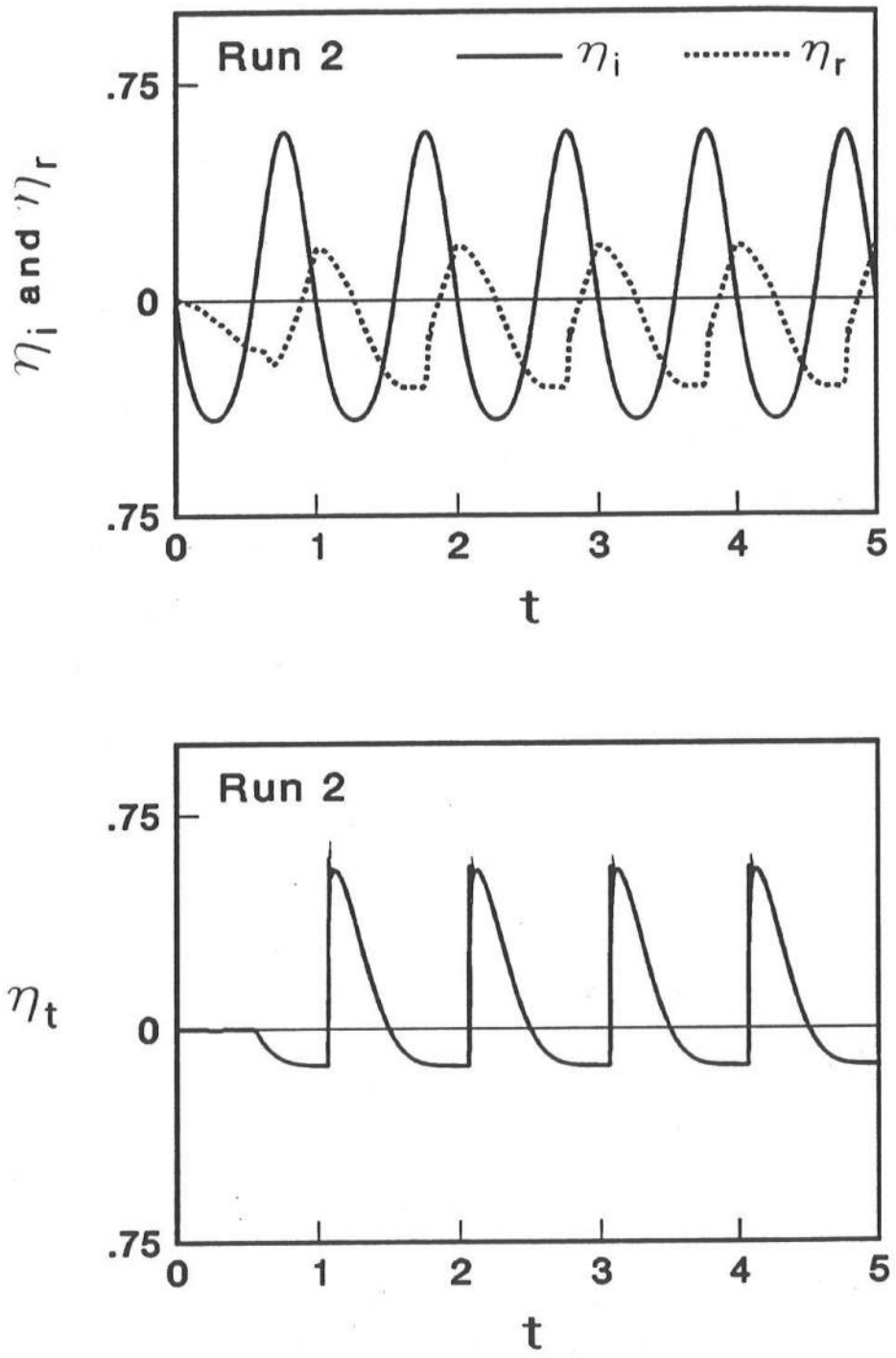

Figure 5. Specified incident wave train $\eta_i(t)$ and computed reflected wave train $\eta_r(t)$ at x=0 as well as computed transmitted wave train $\eta_t(t)$ at $x=x_e$ for Run No. 2.

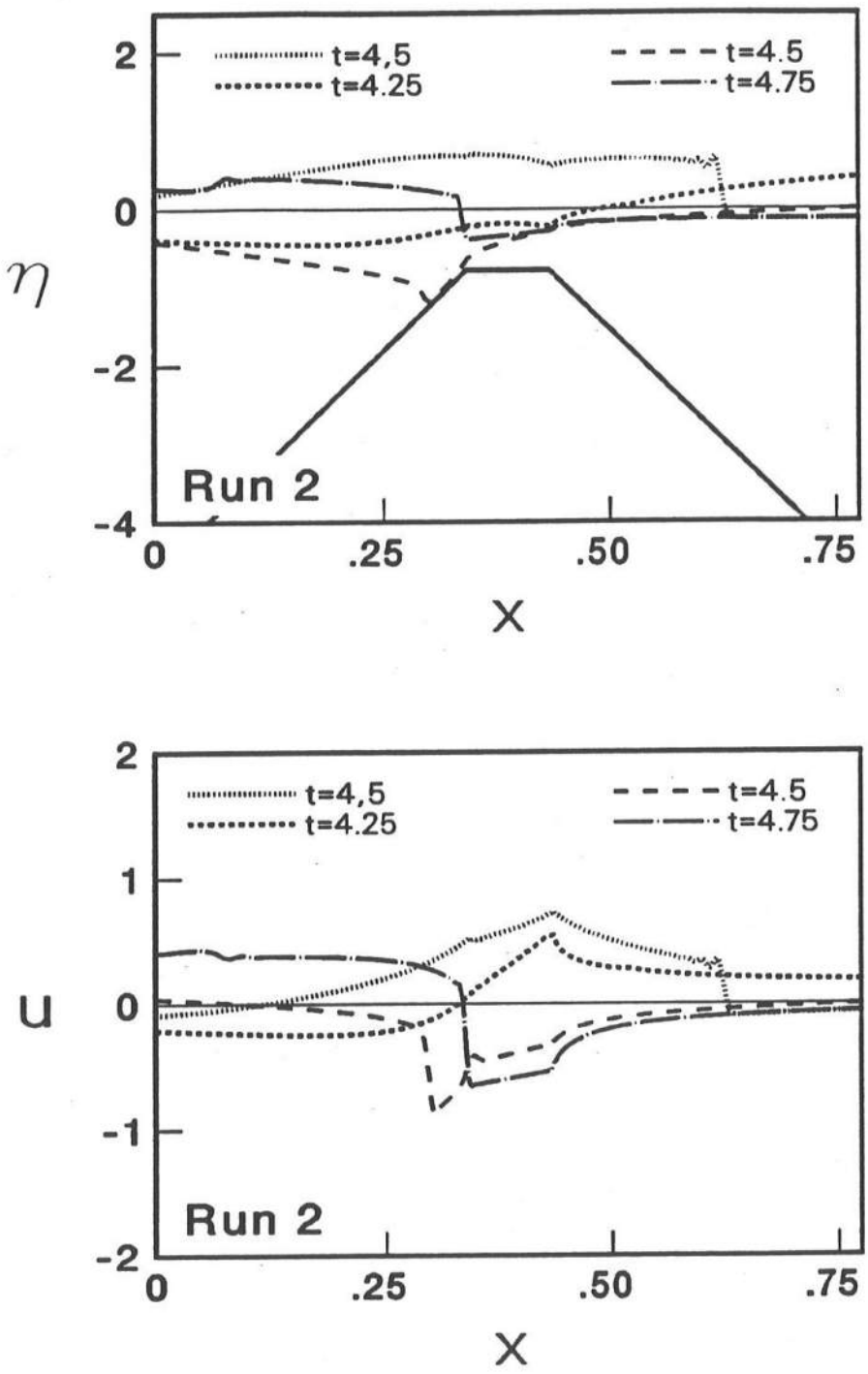

Figure 6. Computed spatial variations of free surface elevation η and horizontal velocity u at t = 4, 4.25, 4.5, 4.75 and 5 for Run No. 2.

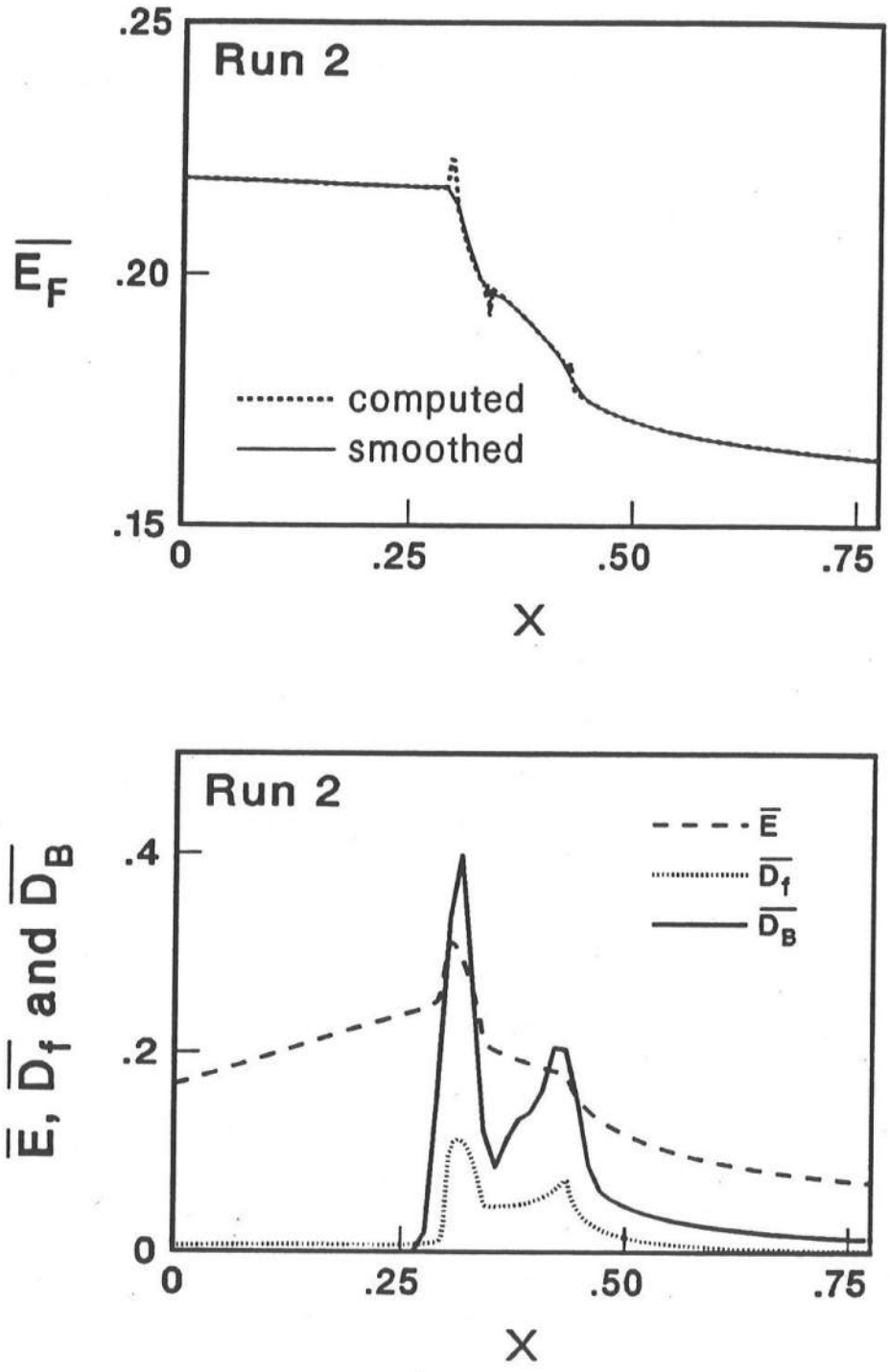

Figure 7. Computed spatial variations of energy flux $\overline{E_F}$, specific energy $\overline{E}$, dissipation rate $\overline{D_f}$ and $\overline{D_B}$ due to bottom friction and wave breaking, respectively, for Run No. 2.

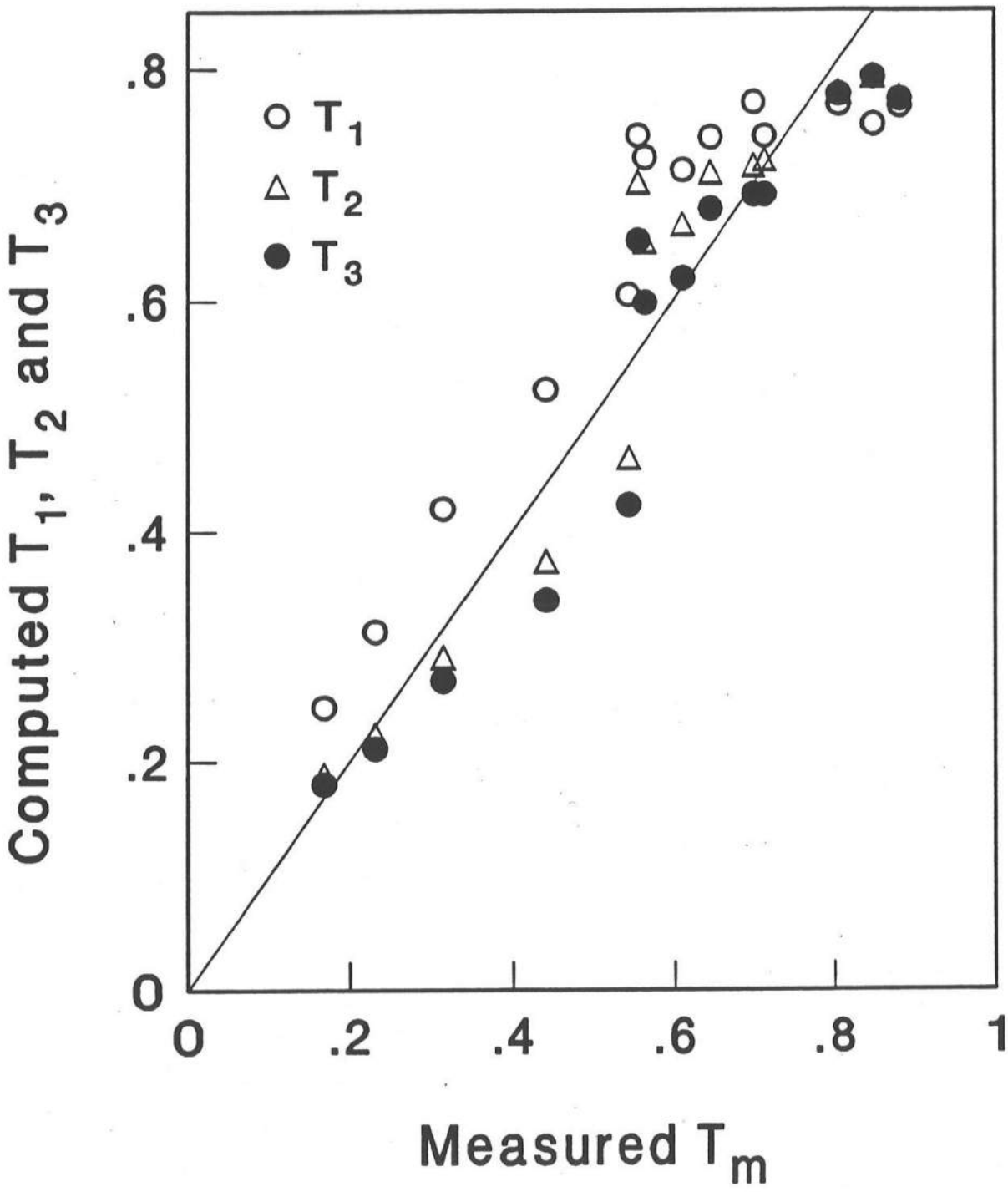

Figure 8. Comparison of computed transmission coefficients T_1, T_2 and T_3 with measured transmission coefficient T_m.

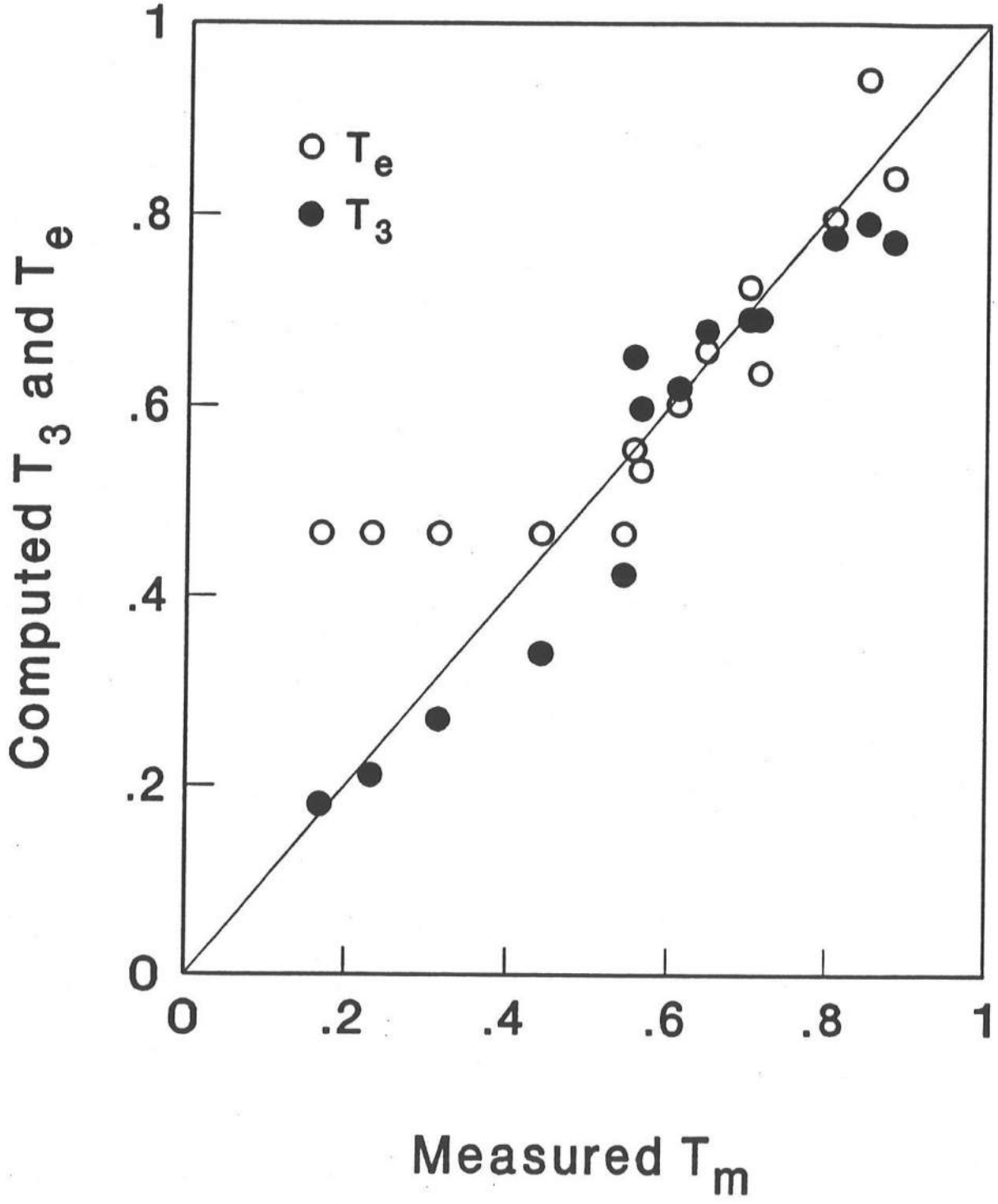

Figure 9. Comparison of computed and empirical transmission coefficients, T_3 and T_e, with measured transmission coefficient T_m.

Measured and Computed Reflection Coefficients

Fig. 10 shows the computed reflection coefficients r_1, r_2 and r_3 compared with the measured reflection coefficient r_m for each of the fourteen runs. The solid line shown in Fig. 10 indicates the perfect agreement. r_2 and r_3 are given by Eqs. 34 and 36, respectively, and based on the reflected wave energy, whereas r_1 given by Eq. 15 is based on the normalized height of the reflected wave train. Since r_3 includes the effect of the wave set-down $\overline{\eta_r}$, $r_3 < r_2$ as indicated in Eq. 36, while r_1 is found to be greater than r_2 for most of the runs as might be discernible in Fig. 10.

The numerical model tends to overestimate the reflection coefficient slightly even if the best estimate r_3 is compared with the measured value r_m. Since the computed and measured transmission coefficients are in agreement, the slight overestimation of the reflection coefficient suggests that the numerical model slightly underestimates the wave energy dissipation due to wave breaking and bottom friction. Increase of the bottom friction factor f' would improve the agreement but may not be warranted without data on the flow field over the submerged breakwater.

Mean Water Level Difference

Fig. 11 shows the computed values of the normalized mean water level difference, $\Delta\bar{\eta}$, as a function of the normalized water depth below SWL, d_c, on the crest of the breakwater. $\Delta\bar{\eta}$ is the difference between the wave setup $\overline{\eta_t}$ at $x=x_e$ and the wave set-down $\overline{\eta_r}$ at $x=0$ as defined in Eq. 17. For each of the fourteen runs, the computed value of $\overline{\eta_r}$ is negative and on the order of magnitude of the positive value of $\overline{\eta_t}$.

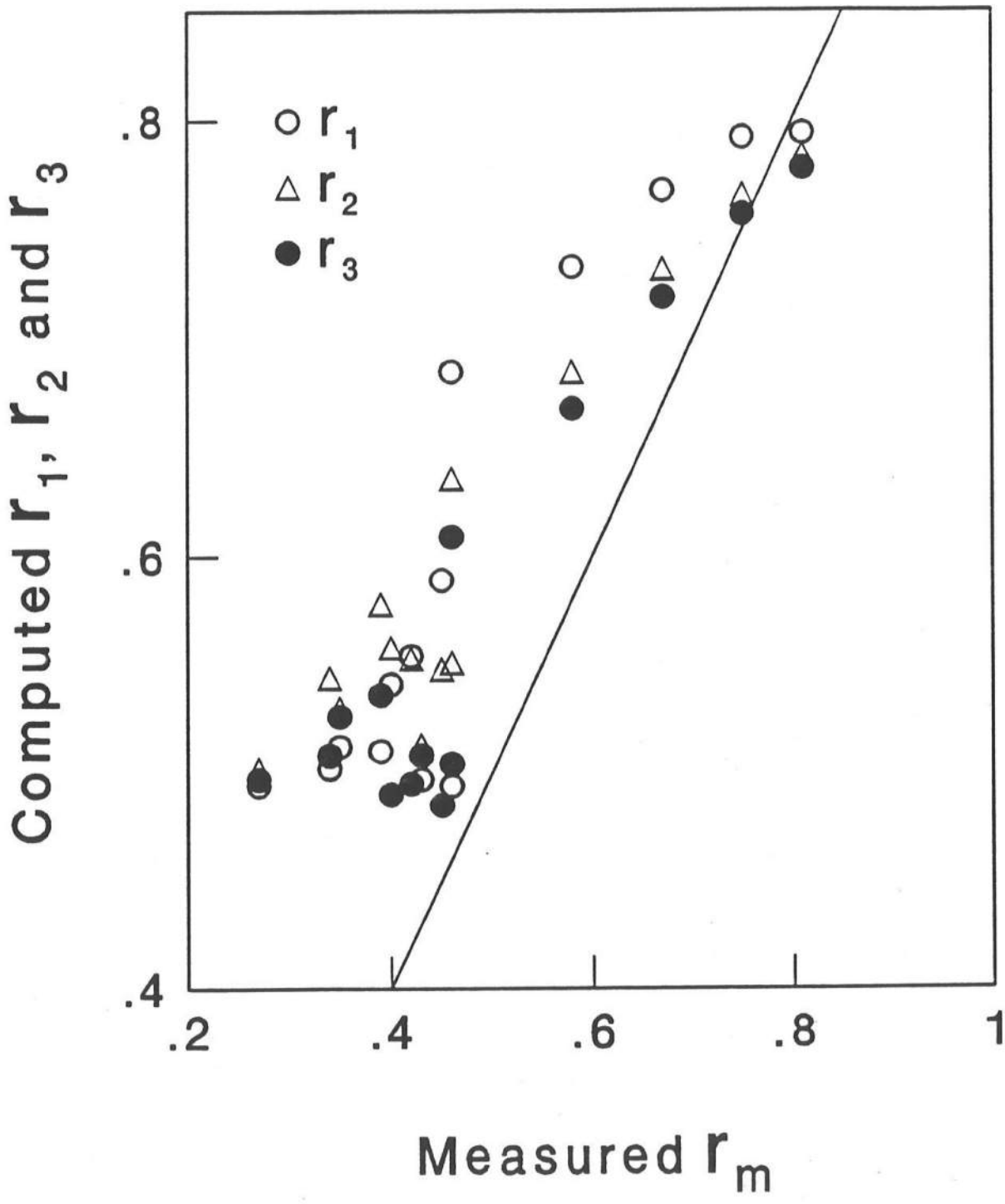

Figure 10. Comparison of computed reflection coefficients r_1, r_2 and r_3 with measured reflection coefficient r_m.

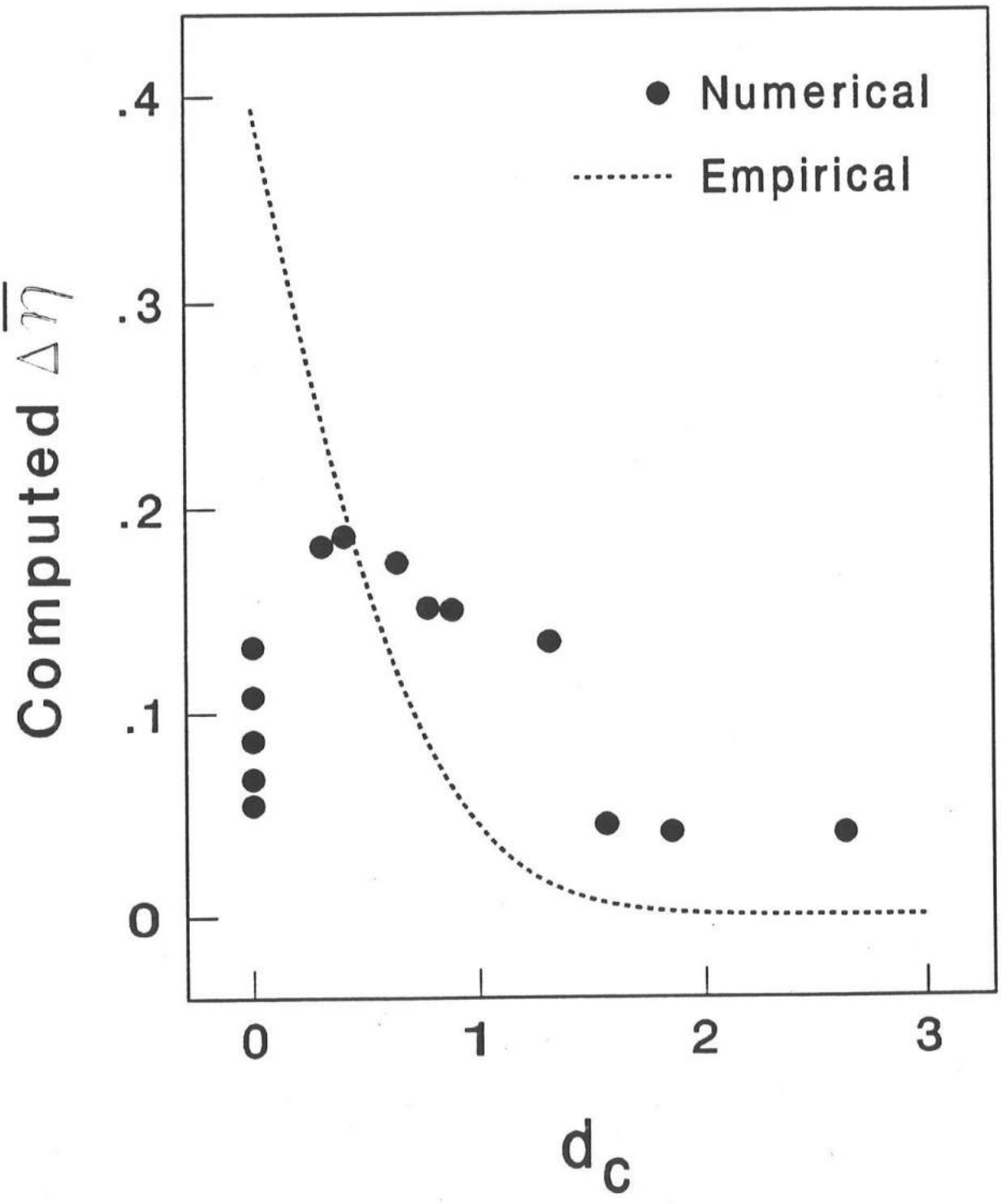

Figure 11. Mean water level difference $\overline{\Delta\eta}$ based on numerical model and empirical formula as a function of d_c.

Since no data on $\Delta\bar{\eta}$ was provided by Seelig (1980), comparison is made with the empirical formula of Diskin et al. (1970) for ponding behind low and submerged permeable breakwaters which are completely enclosed. The comparison is only qualitative since this formula corresponds to the case of no net volume flux, that is, $\bar{m} = 0$. This empirical formula can be expressed as

$$\Delta\bar{\eta} = 0.6\ (K_s)^{-1}\ \exp[-(0.7 + K_s d_c)^2] \tag{40}$$

in which K_s = shoaling coefficient at x=0 based on linear wave theory. The dotted line shown in Fig. 11 corresponds to Eq. 40 where $K_s = 0.932$ for all the runs listed in Table 1. The computed values of $\Delta\bar{\eta}$ are on the same order of magnitude as those based on Eq. 40 as long as d_c is not too small. If the crest of the breakwater is located near SWL, $\Delta\bar{\eta}$ is expected to be strongly influenced by the permeability of a breakwater and whether the water behind the breakwater is allowed to escape landward or laterally.

In addition, $\Delta\bar{\eta}$ is calculated using the analytical solution derived by Longuet-Higgins (1967) which can be expressed as

$$\Delta\bar{\eta} = \pi(1 + r_m^2 - T_m^2)\ \left[4Ld_t\ \sinh\left(\frac{4\pi}{L}\right)\right]^{-1} \tag{41}$$

in which the measured reflection and transmission coefficients are used to calculate the value of $\Delta\bar{\eta}$ for each of the fourteen runs listed in Table 1. Eq. 41 predicts the values of $\Delta\bar{\eta}$ in the range $0.0003 \leq \Delta\bar{\eta} \leq 0.0095$ which are much smaller than those predicted by the numerical model. Eq. 41 is based on the assumption that the motion everywhere is irrotational and is not applicable if wave breaking occurs. For breaking waves, Dalrymple and Dean (1971) performed an analysis similar to that used for predicting wave set-down and set-up on a beach and obtained reasonable agreement with the data of Diskin et al. (1970).

Time-Averaged Volume Flux

Fig. 12 shows the computed values of the normalized time-averaged volume flux per unit width, $\bar{m}$, as a function of d_c. The value of $\bar{m}$ in the absence of the breakwater based on Stokes second-order theory (e.g., Dean and Dalrymple, 1984), which is given by $\bar{m} = [\sigma/(8d_t L)]$ in the present notation, is also plotted in Fig. 12 for each run. Fig. 12 indicates that the presence of the breakwater will increase the net volume flux especially if d_c is small.

Available data on wave overtopping rates such as that given in SPM appears to be limited to subaerial breakwaters because of the ease of instrumentation. The empirical formula for wave overtopping given in SPM may be used to estimate the value of $\bar{m}$ if d_c is zero or negative. For the case of $d_c = 0$, this formula reduces to $\bar{m} = (\sqrt{Q_0^*}\, K_s^{-1.5})$ in which Q_0^* = empirical coefficient and $K_s = 0.932$ for all the runs. The value of Q_0^* for a 1:1.5 smooth slope on a 1:10 nearshore slope is listed as a function of $(K_s d_t)$ and $(K_s \sigma^2)^{-1}$ in SPM. For the runs with $d_c = 0$ listed in Table 1, Q_0^* may range from 0.007 to 0.088, resulting in $\bar{m} = 0.09 - 0.33$. This range is comparable with the order of magnitude associated with the computed values of $\bar{m}$ shown in Fig. 12.

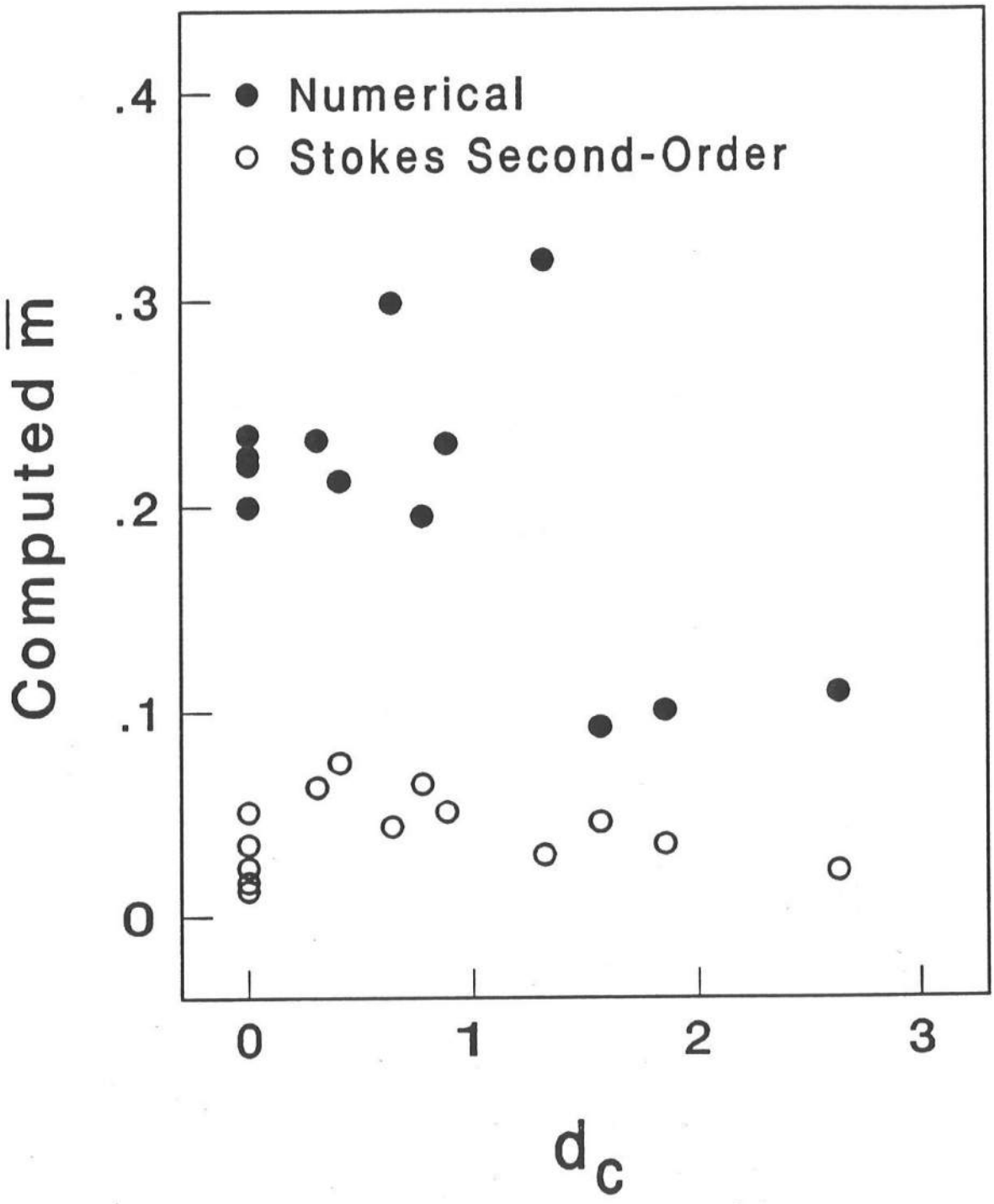

Figure 12. Time-averaged volume flux $\bar{m}$ based on numerical model and Stokes second-order theory as a function of d_c.

PART V: CONCLUSIONS

A numerical model is presented to examine the hydrodynamic processes involved in monochromatic wave reflection, breaking and transmission over a submerged impermeable breakwater. The numerical model is shown to be in agreement with a set of data on wave reflection and transmission coefficients. It is also shown to predict the mean water level difference and net volume flux per unit width which are in qualitative agreement with limited information available at present.

The numerical model may be used to provide the hydrodynamic quantities needed for the design of a submerged breakwater as well as to interpret hydraulic model test results since some hydrodynamic quantities such as the rate of wave energy dissipation are extremely difficult to measure directly.

However, the numerical model needs to be expanded to include the permeability of a breakwater and the randomness of incident wind waves even under the assumption of normally incident waves on a long breakwater. In addition, comprehensive and detailed measurements will be required to calibrate and evaluate such an expanded numerical model. Improvement of our numerical prediction capabilities may stimulate improvement of our experimental capabilities.

REFERENCES

Adams, C.B. and Sonu, C.J. (1986). "Wave transmission across submerged near-surface breakwaters." Proc. 20th Coast. Engrg. Conf., ASCE, 2, 1729-1738.

Ahrens, J.P. (1987). "Characteristics of reef breakwaters." Tech. Rept. CERC-87-17, U.S. Army Coast. Engrg. Res. Ctr., Vicksburg, Miss.

Dalrymple, R.A. and Dean, R.G. (1971). Discussion on "Piling-up behind low and submerged permeable breakwaters." J. Wtrways. Harbors Div., ASCE, 97(WW2), 423-427.

Dean, R.G. and Dalrymple, R.A. (1984). Water Wave Mechanics for Engineers and Scientists, Prentice-Hall, Englewood Cliffs, N.J.

Diskin, M.H., Vajda, M.L. and Amir, I. (1970). "Piling-up behind low and submerged permeable breakwaters." J. Wtrways. Harbors Div., ASCE, 96(WW2), 359-372.

Goda, Y. and Suzuki, Y. (1976). "Estimation of incident and reflected waves in random wave experiments." Proc. 15th Coast. Engrg. Conf., ASCE, 1, 828-845.

Henderson, F.M. (1966). Open Channel Flow. Macmillan, New York, N.Y.

Kobayashi, N., DeSilva, G.S. and Watson, K.D. (1989). "Wave transformation and swash oscillation on gentle and steep slopes." J. Geophys. Res., 94(C1), 951-966.

Kobayashi, N., Otta, A.K. and Roy, I. (1987). "Wave reflection and run-up on rough slopes." J. Wtrway. Port Coast. Oc. Engrg., ASCE, 113(3), 282-298.

Kobayashi, N. and Watson, K.D. (1987). "Wave reflection and runup on smooth slopes." Proc. Coast. Hydrodynamics, ASCE, 548-563.

Kobayashi, N. and Wurjanto, A. (1988). "Numerical prediction of wave overtopping on coastal structures." Res. Report No. CE-88-72, Dept. of Civil Engrg., Univ. of Delaware, Newark, Delaware.

Kobayashi, N. and Wurjanto, A. (1989a). "Wave overtopping on coastal structures." J. Wtrway. Port Coast. Oc. Engrg., ASCE, 115(2), 235-251.

Kobayashi, N. and Wurjanto, A. (1989b). "Wave overtopping and transmission over breakwaters." Proc. PORT'S 89, ASCE (in press).

Kobayashi, N. and Wurjanto, A. (1989c). "Wave transmission over submerged breakwaters." J. Wtrway. Port Coast. Oc. Engrg., ASCE (in press).

Longuet-Higgins, M.S. (1967). "On the wave-induced difference in mean sea level between the two sides of a submerged breakwater." J. Marine Res., 25(2), 148-153.

Longuet-Higgins, M.S. and Cokelet, E.D. (1976). "The deformation of steep surface waves on water. I. A numerical method of computation." Proc. R. Soc. Lond., A(350), 1-26.

Peregrine, D.H. (1966). "Calculations of the development of an undular bore." J. Fluid Mech., 25(2), 321-330.

Seelig, W.N. (1980). "Two-dimensional tests of wave transmission and reflection characteristics of laboratory breakwaters." Tech. Rept. No. 80-1, U.S. Army Coast. Engrg. Res. Ctr., Fort Belvoir, Va.

U.S. Army Coastal Engineering Research Center (1984). Shore Protection Manual, 2, Government Printing Office, Washington, D.C.

APPENDIX A: NOTATION

The following symbols are used in this report:

a_1 = 0.5;

a_2 = normalized amplitude of Stokes second-order harmonic;

B' = dimensional crest width of submerged breakwater;

c = $\sqrt{h}$;

d_c = water depth below SWL on crest of submerged breakwater;

d_e = water depth below SWL at landward boundary;

d_t = water depth below SWL at seaward boundary;

D_B = rate of energy dissipation per unit horizontal area due to wave breaking;

D_f = rate of energy dissipation per unit horizontal area due to bottom friction;

E = specific energy defined as sum of kinetic and potential energy per unit horizontal area;

E_F = energy flux per unit width;

f = bottom friction factor;

g = gravitational acceleration;

H' = dimensional wave height at seaward boundary;

h = instantaneous water depth;

h'_s = dimensional height of submerged breakwater;

K_s = shoaling coefficient at seaward boundary;

L = wavelength at seaward boundary;

m = normalized volume flux per unit width;

Q_o^* = empirical coefficient for wave overtopping formula;

R' = dimensional wave run-up on seaward slope of breakwater in absence of wave transmission;

r_m = measured wave reflection coefficient;

r_1 = wave reflection coefficient computed using Eq. 15;

r_2 = wave reflection coefficient computed using Eq. 34;

r_3 = wave reflection coefficient computed using Eq. 36;

T' = dimensional wave period;

T_e = wave transmission coefficient based on empirical formula given by Eq. 39;

T_m = measured wave transmission coefficient;

T_1 = wave transmission coefficient computed using Eq. 16;

T_2 = wave transmission coefficient computed using Eq. 35;

T_3 = wave transmission coefficient computed using Eq. 37;

t = time;

t_o = time shift introduced to make $\eta_i = 0$ at $t = 0$;

t_p = time when flow field in computation domain becomes periodic;

U_r = Ursell parameter at seaward boundary;

u = instantaneous depth-averaged horizontal velocity;

u_i = horizontal velocity at $x = 0$ due to incident wave;

u_r = horizontal velocity at $x = 0$ due to reflected wave;

x = horizontal coordinate with $x = 0$ at seaward boundary;

x_e = x-coordinate at landward boundary;

z = vertical coordinate with $z = 0$ at SWL;

α = characteristic variable defined as $\alpha = (u + 2c)$;

β = characteristic variable defined as $\beta = (-u + 2c)$;

η = instantaneous free surface elevation above SWL;

η_i = free surface variation of incident wave train at $x = 0$;

η_r = free surface variation of reflected wave train at $x = 0$;

η_t = free surface variation of transmitted wave train at $x = x_e$;

$\Delta\bar{\eta}$ = mean water level difference between set-up $\bar{\eta}_t$ at $x = x_e$ and set-down $\overline{\eta_r}$ at $x = 0$;

θ = local slope angle or gradient;

ξ = surf similarity parameter in absence of wave transmission;

ρ = fluid density; and

σ = dimensionless parameter related to wave steepness.

Superscript

$'$ = indicator for physical variables; and

$\bar{}$ = indicator for time averaging during $t_p \leq t \leq (t_p + 1)$.

APPENDIX B: COMPUTED RESULTS FOR 14 RUNS

The computed results for the fourteen runs listed in Table 1 are presented herein. The specified incident wave train $\eta_i(t)$ at $x = 0$, the computed reflected wave train $\eta_r(t)$ at $x = 0$, and the computed transmitted wave train $\eta_t(t)$ at $x = x_e$ for Run No. I are plotted as a function of the normalized time t in the range $0 \leq t \leq 5$ in page B-2I with $I = 1,2,\ldots,14$.

On the other hand, the computed spatial variations of the normalized free surface elevation η and the normalized horizontal velocity u in the range $0 \leq x \leq x_e$ at $t = 4$, 4.25, 4.5, 4.75 and 5 for Run No. I are plotted in page B-(2I+1) with $I = 1,2,\ldots,14$.

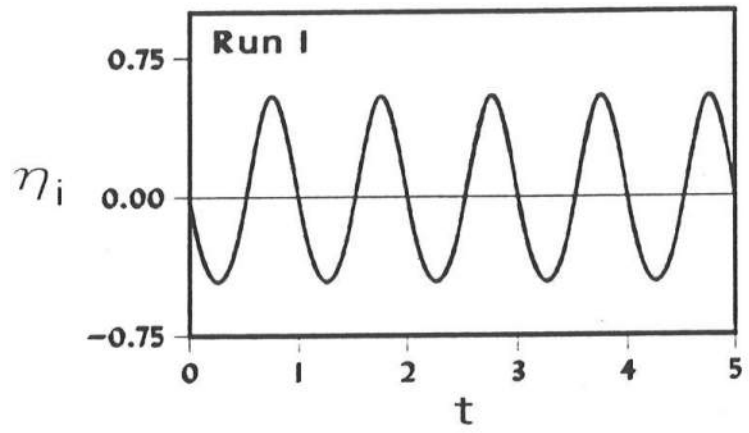
Run 1
0.75
0.00
−0.75
η_i
0
1
2
3
4
5
t

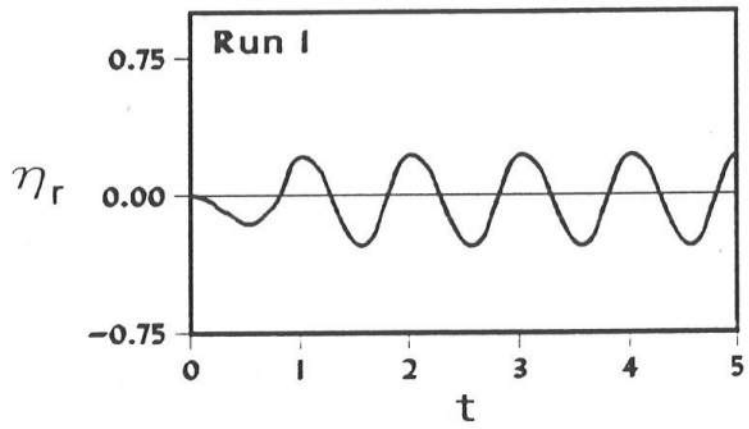
Run 1
0.75
0.00
−0.75
η_r
0
1
2
3
4
5
t

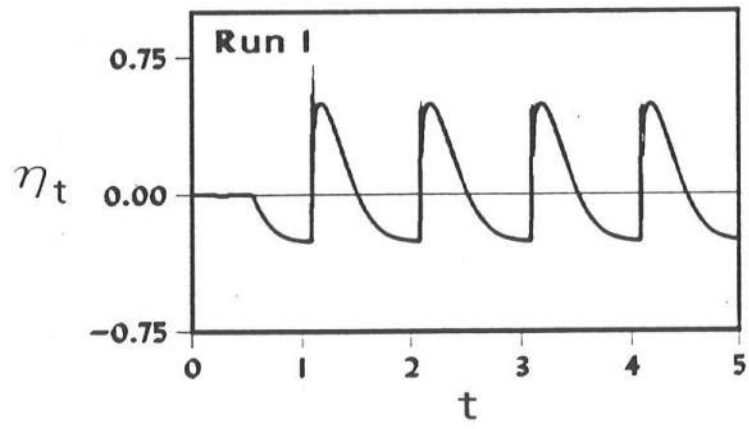
Run 1
0.75
0.00
−0.75
η_t
0
1
2
3
4
5
t

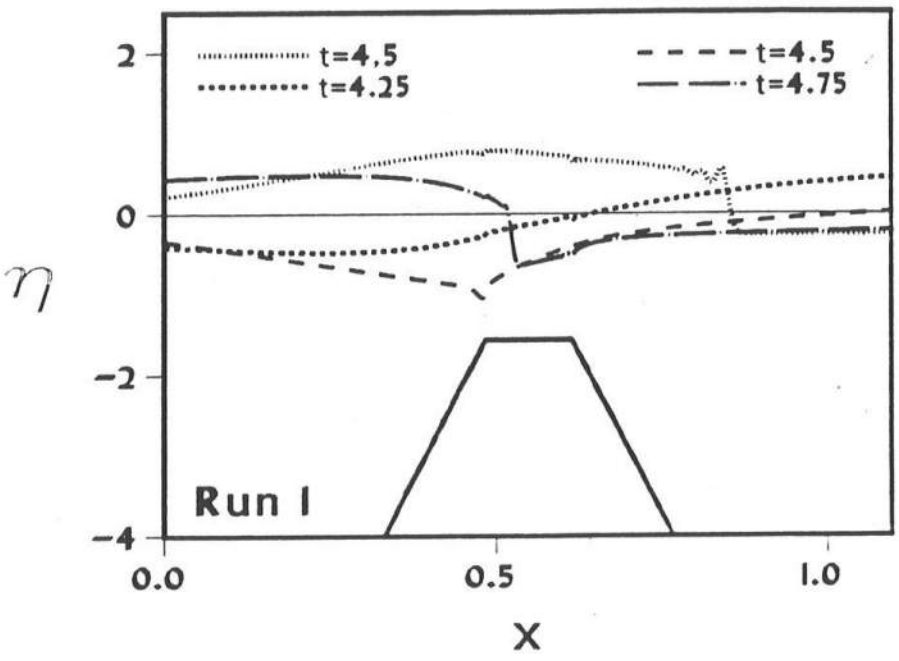
t=4,5
t=4.25
t=4.5
t=4.75
2
0
−2
−4
η
Run I
0.0
0.5
1.0
X

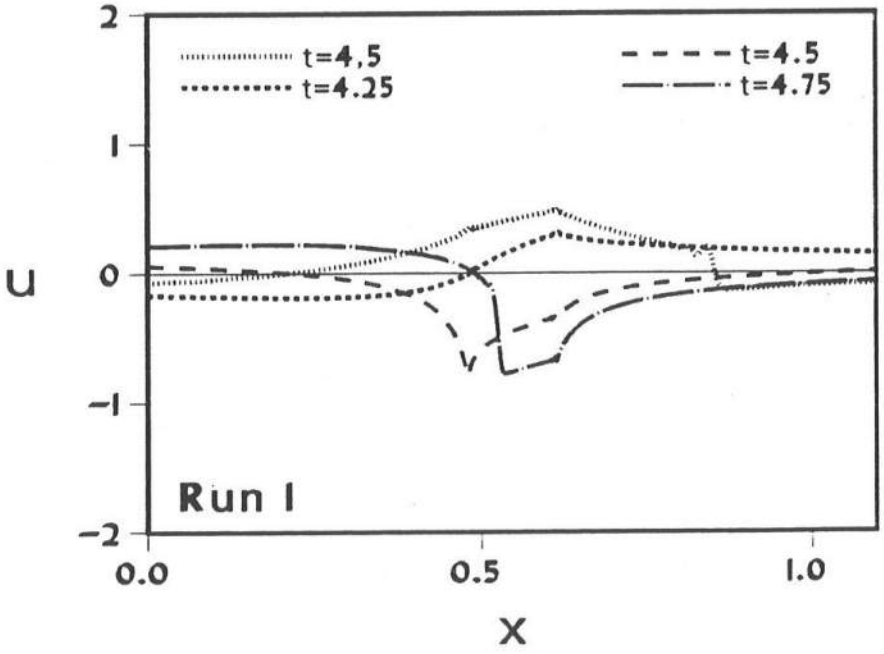
t=4,5
t=4.25
t=4.5
t=4.75
2
1
0
−1
−2
u
Run I
0.0
0.5
1.0
X

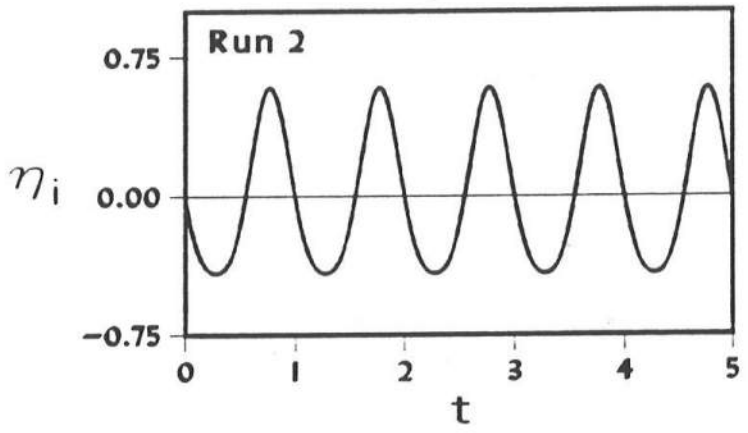
Run 2
0.75
η_i
0.00
−0.75
0
1
2
3
4
5
t

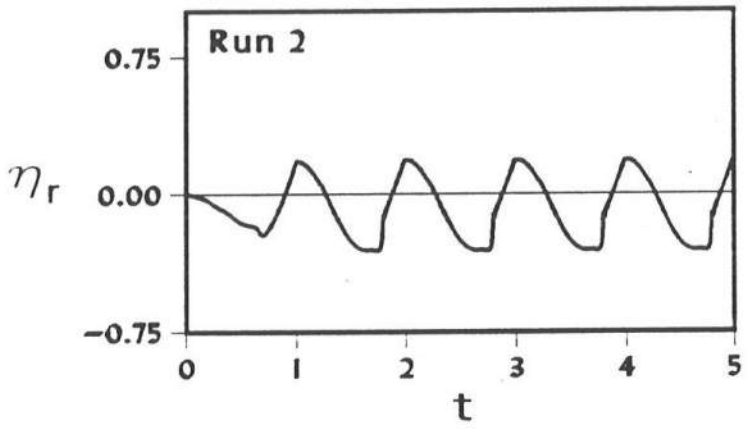
Run 2
0.75
η_r
0.00
−0.75
0
1
2
3
4
5
t

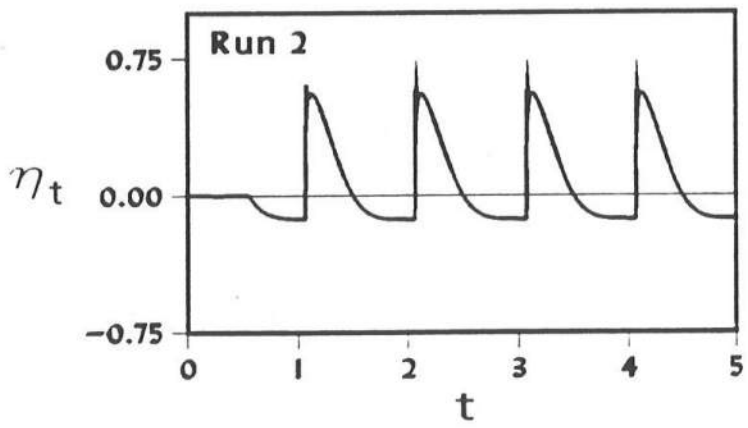
Run 2
0.75
η_t
0.00
−0.75
0
1
2
3
4
5
t

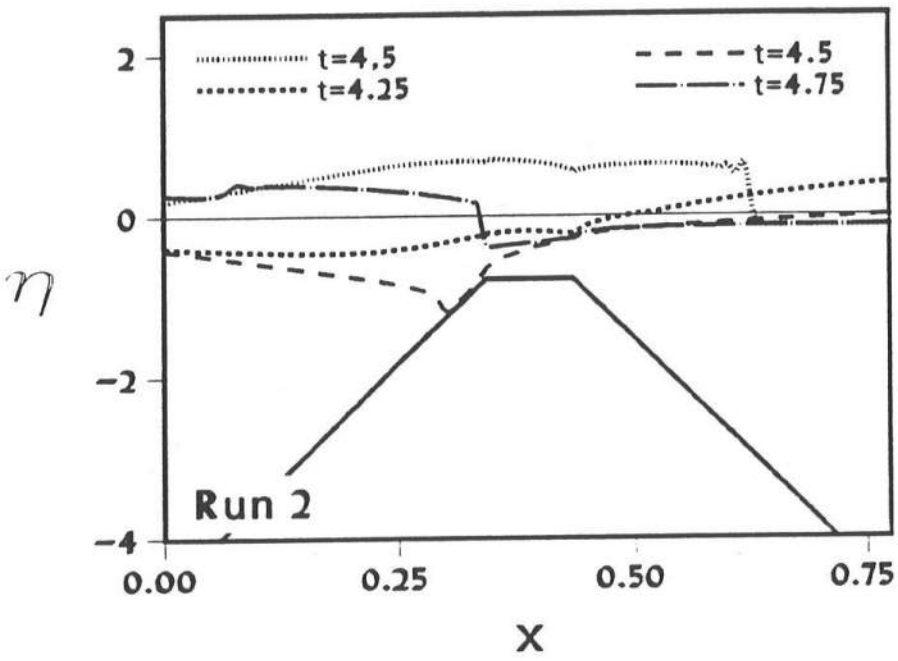
t=4,5
t=4.25
t=4.5
t=4.75
2
0
−2
−4
η
Run 2
0.00
0.25
0.50
0.75
X

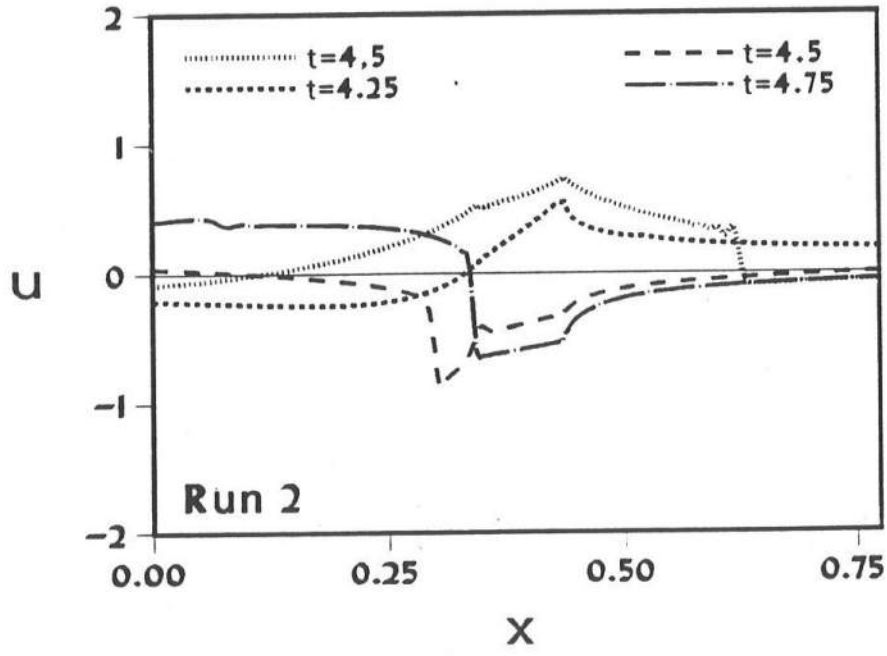
t=4,5
t=4.25
t=4.5
t=4.75
2
1
0
−1
−2
u
Run 2
0.00
0.25
0.50
0.75
X

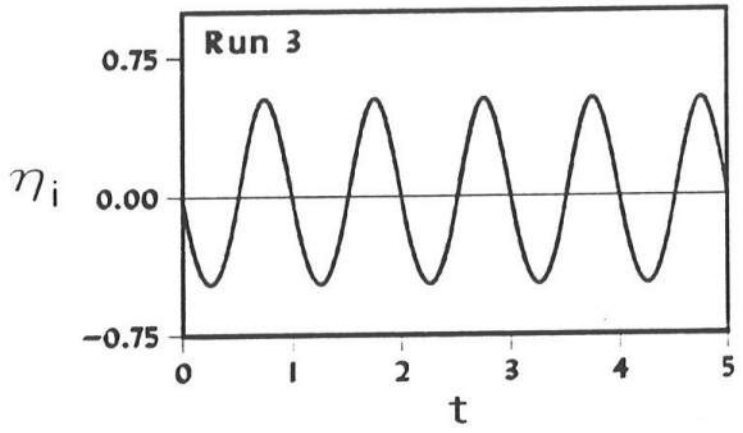
Run 3
0.75
0.00
−0.75
η_i
0
1
2
3
4
5
t

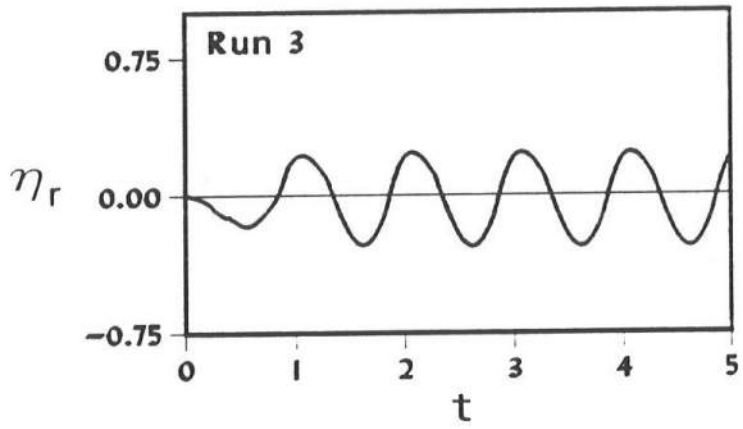
Run 3
0.75
0.00
−0.75
η_r
0
1
2
3
4
5
t

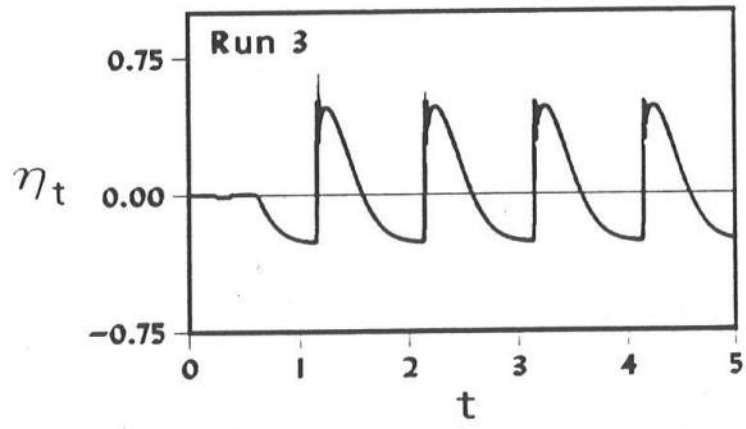
Run 3
0.75
0.00
−0.75
η_t
0
1
2
3
4
5
t

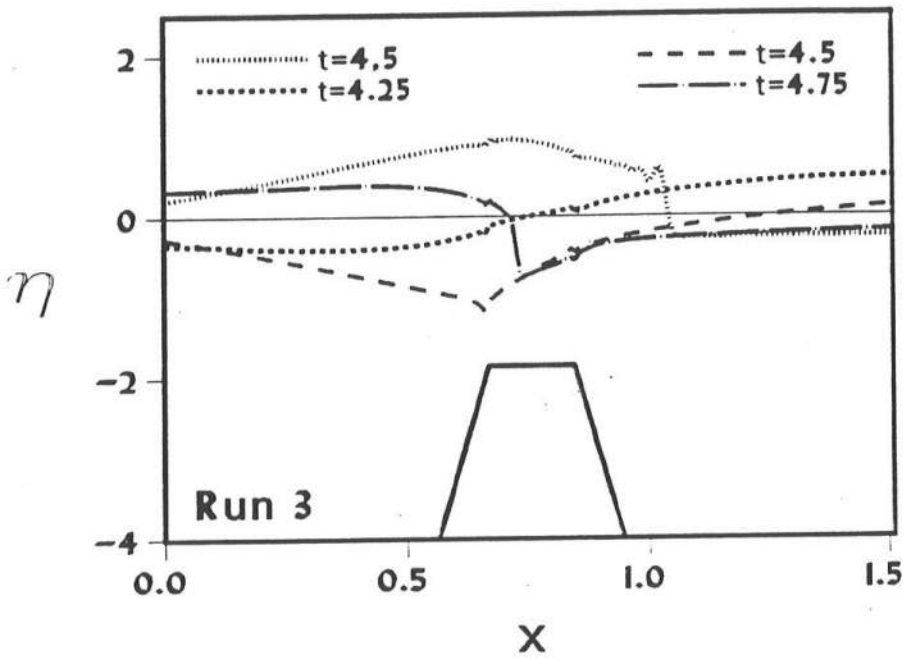
t=4.5
t=4.25
t=4.5
t=4.75
2
0
−2
−4
η
Run 3
0.0
0.5
1.0
1.5
X

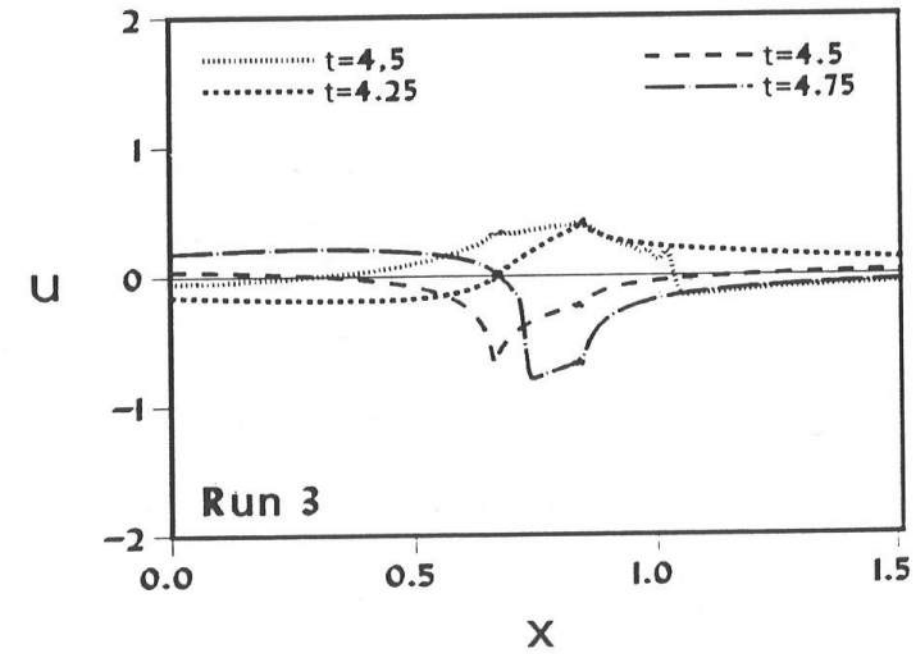
t=4.5
t=4.25
t=4.5
t=4.75
2
1
0
−1
−2
u
Run 3
0.0
0.5
1.0
1.5
X

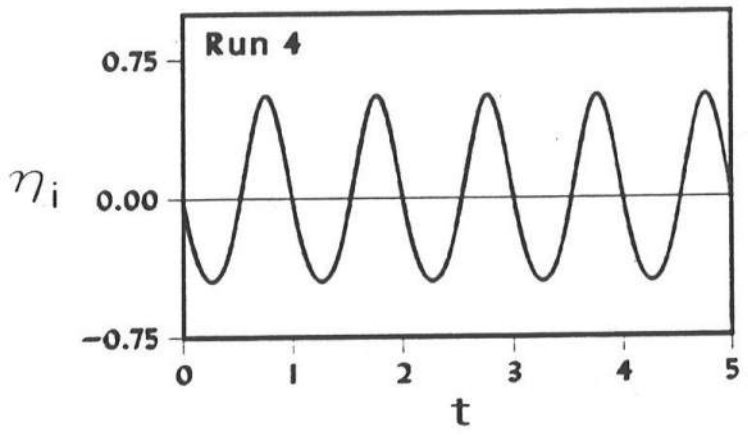
Run 4
0.75
0.00
−0.75
η_i
0
1
2
3
4
5
t

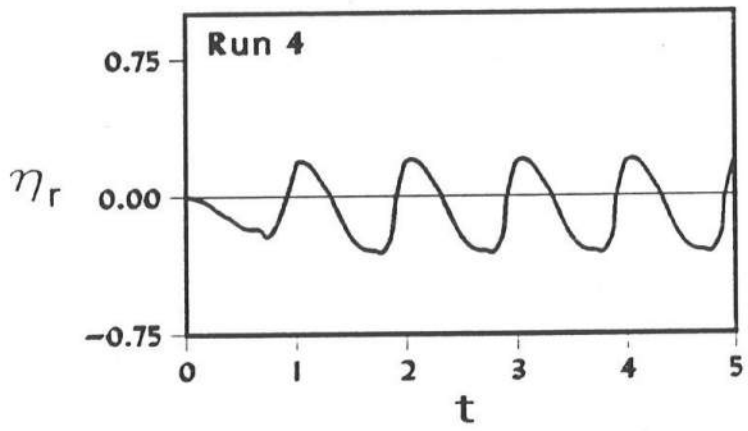
Run 4
0.75
0.00
−0.75
η_r
0
1
2
3
4
5
t

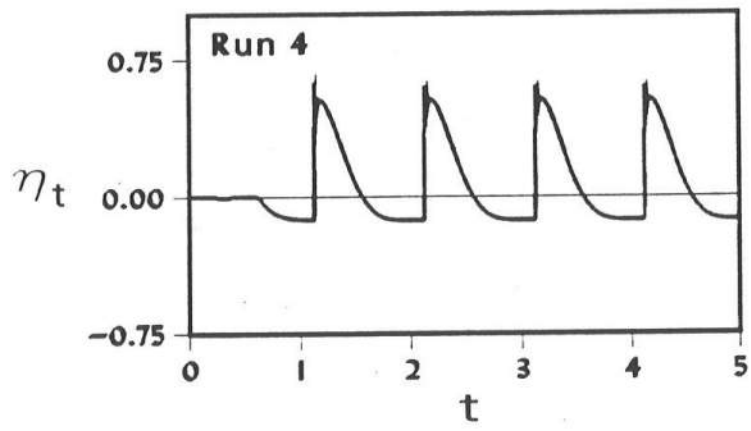
Run 4
0.75
0.00
−0.75
η_t
0
1
2
3
4
5
t

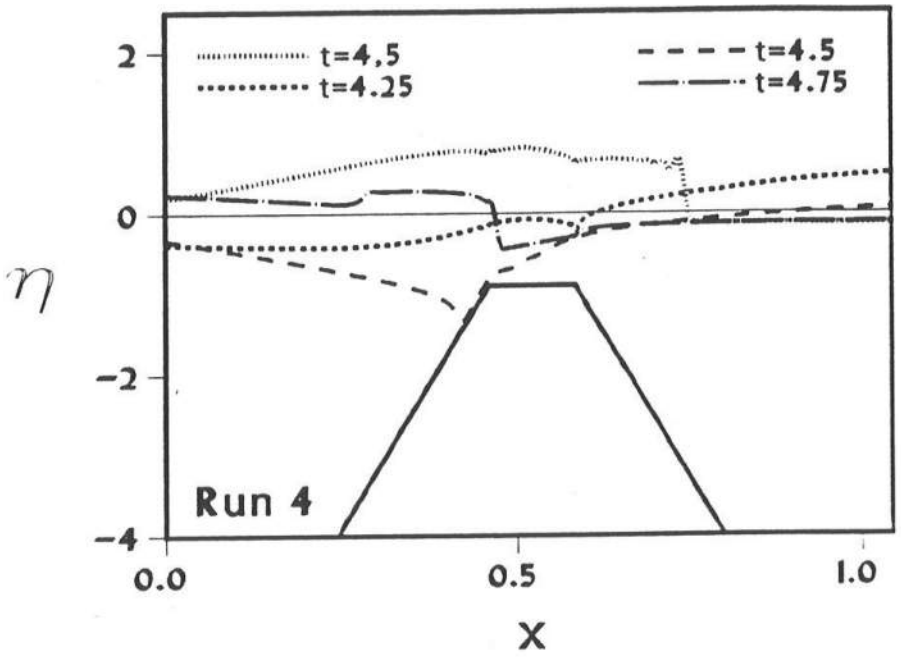
t=4,5
t=4.25
t=4.5
t=4.75
2
0
−2
−4
η
Run 4
0.0
0.5
1.0
X

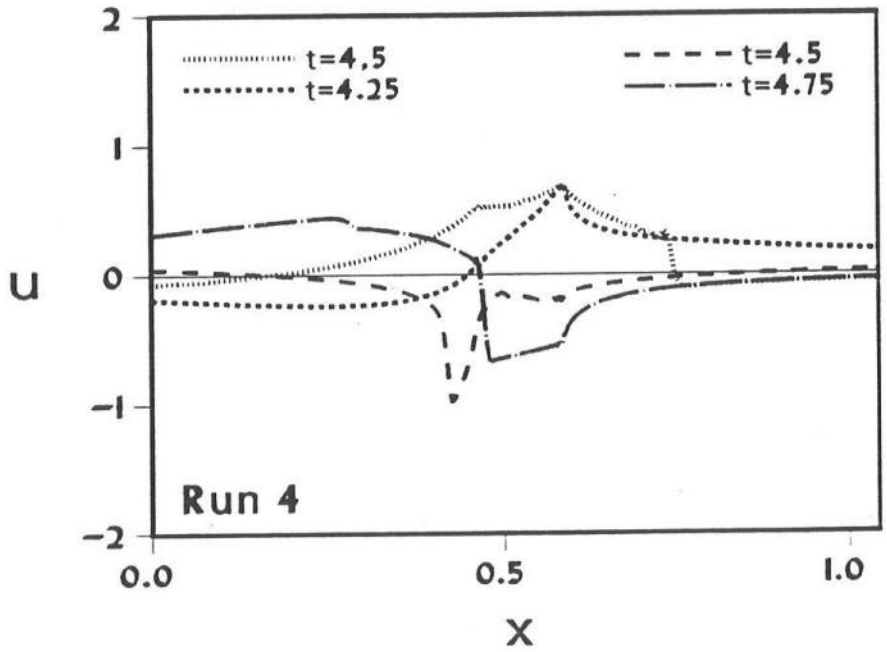
t=4,5
t=4.25
t=4.5
t=4.75
2
1
0
−1
−2
u
Run 4
0.0
0.5
1.0
X

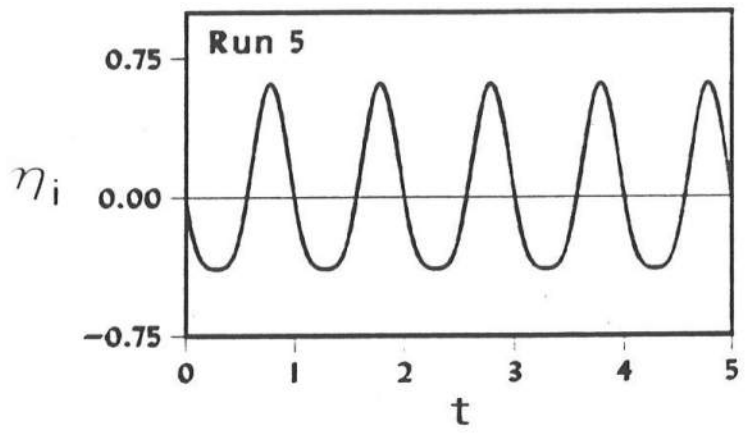
Run 5
0.75
0.00
−0.75
η_i
0
1
2
3
4
5
t

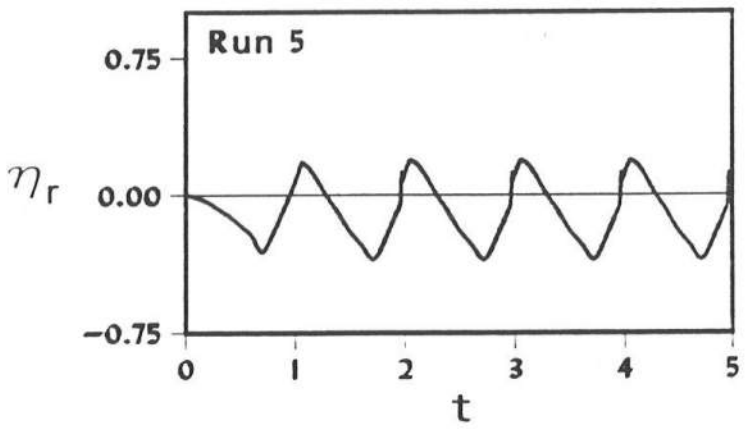
Run 5
0.75
0.00
−0.75
η_r
0
1
2
3
4
5
t

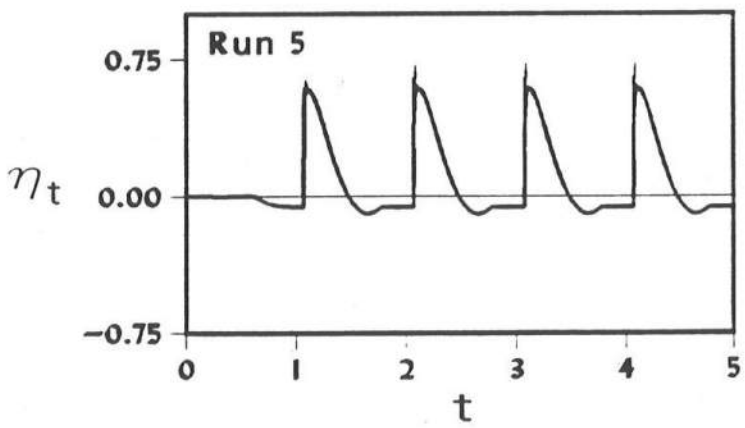
Run 5
0.75
0.00
−0.75
η_t
0
1
2
3
4
5
t

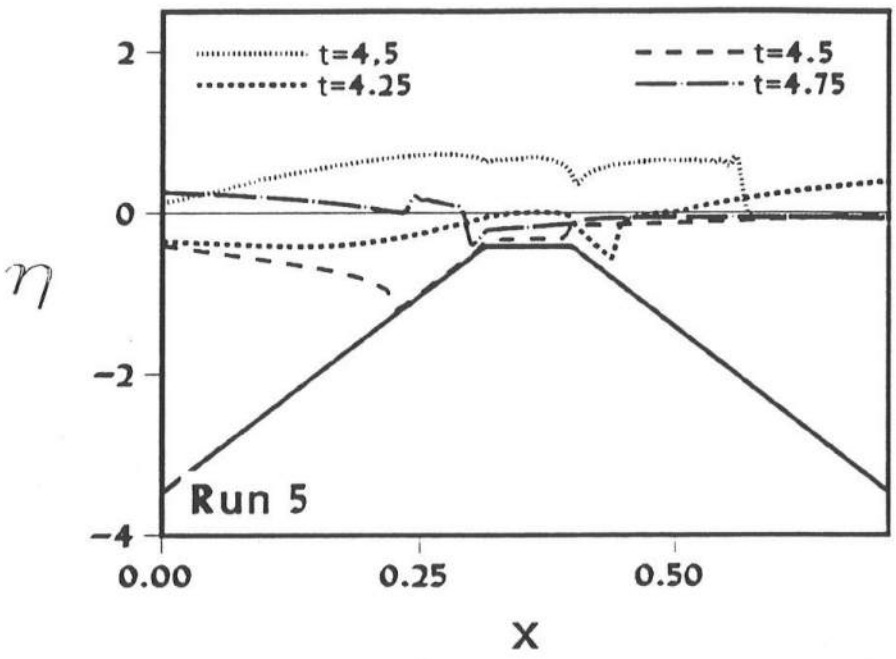
t=4,5
t=4.25
t=4.5
t=4.75
2
0
−2
−4
η
Run 5
0.00
0.25
0.50
X

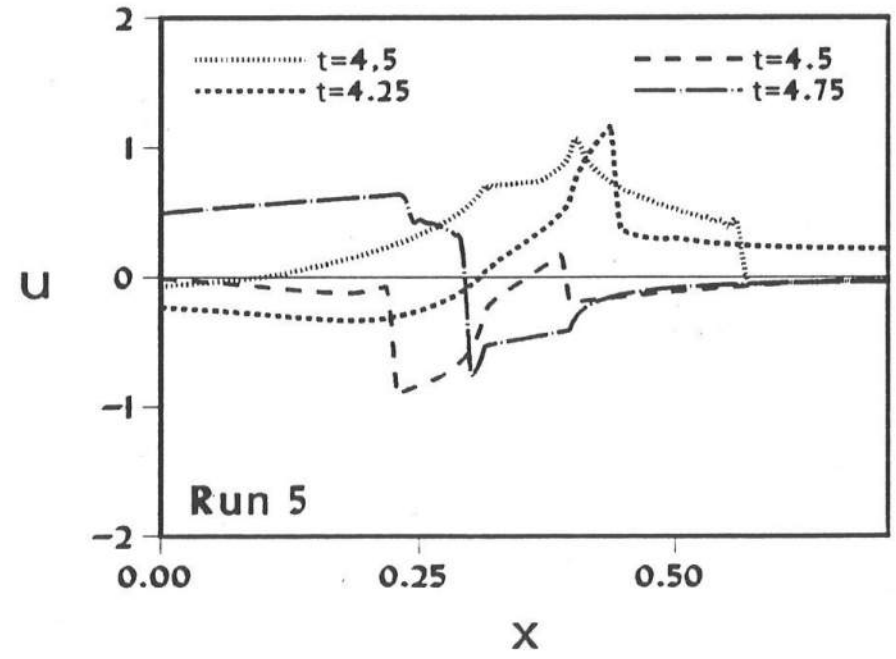
t=4,5
t=4.25
t=4.5
t=4.75
2
1
0
−1
−2
u
Run 5
0.00
0.25
0.50
X

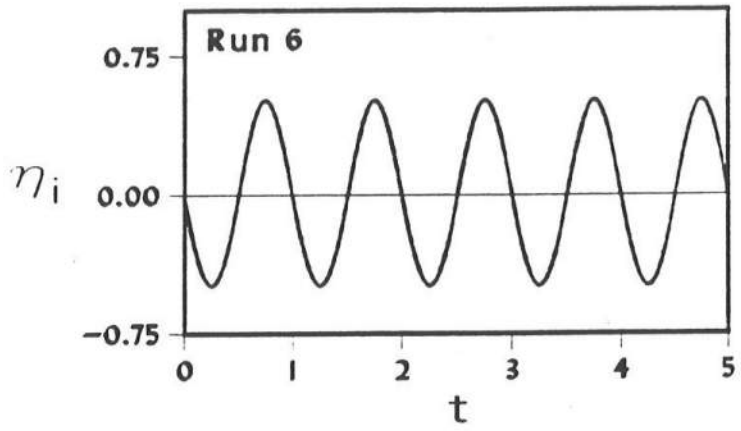
Run 6
0.75
0.00
−0.75
η_i
0
1
2
3
4
5
t

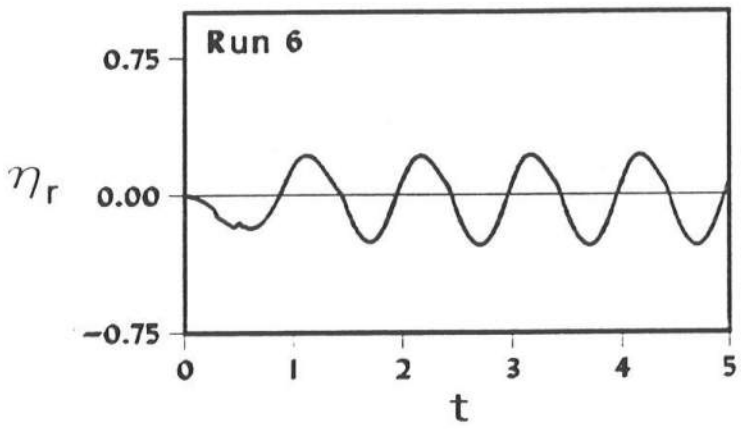
Run 6
0.75
0.00
−0.75
η_r
0
1
2
3
4
5
t

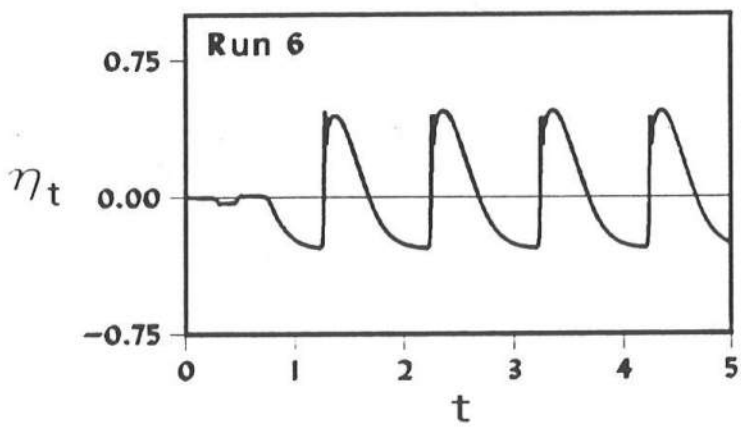
Run 6
0.75
0.00
−0.75
η_t
0
1
2
3
4
5
t

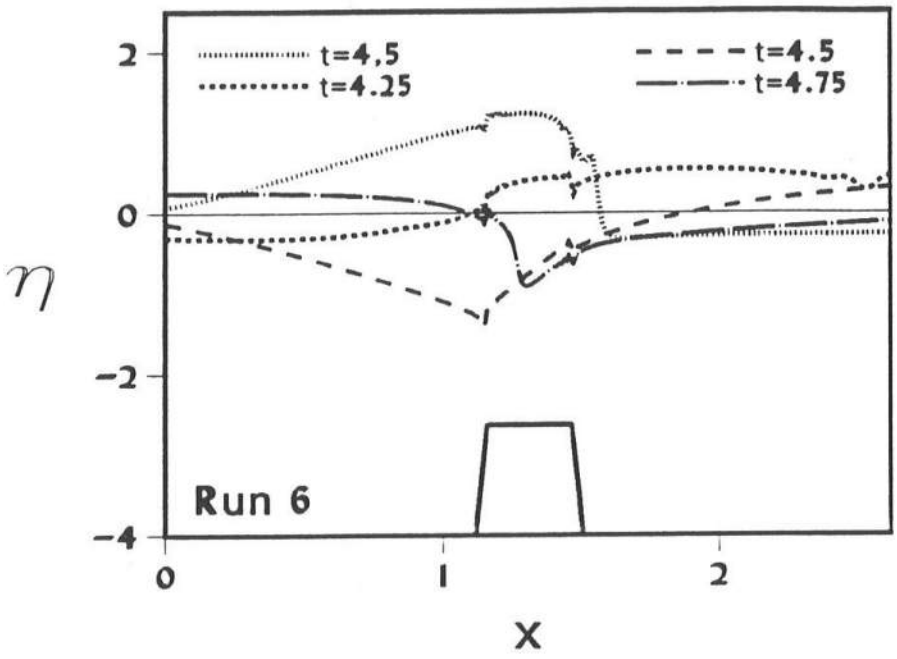
t=4.5
t=4.25
t=4.5
t=4.75
Run 6
η
X

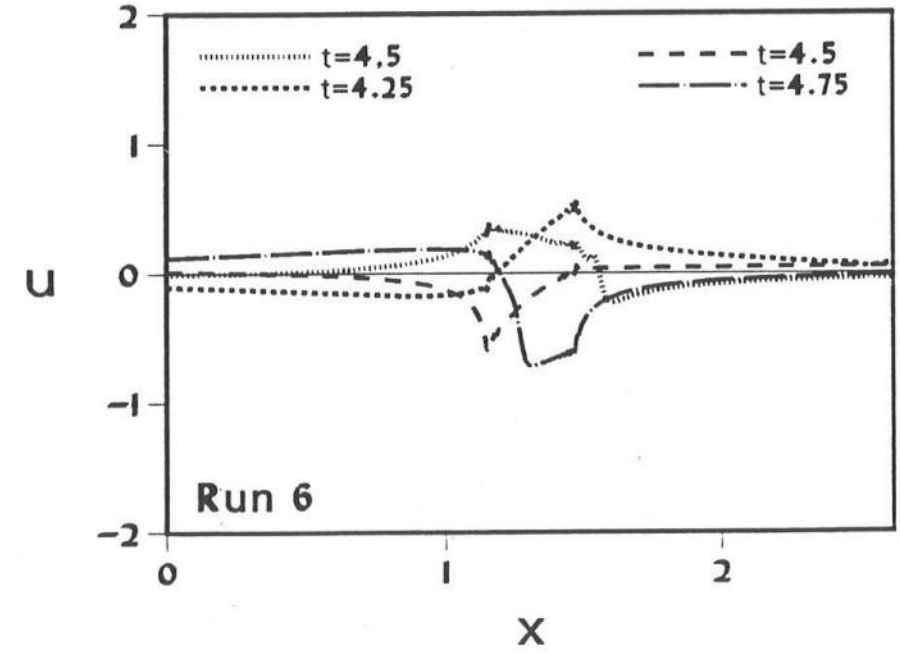
t=4.5
t=4.25
t=4.5
t=4.75
Run 6
u
X

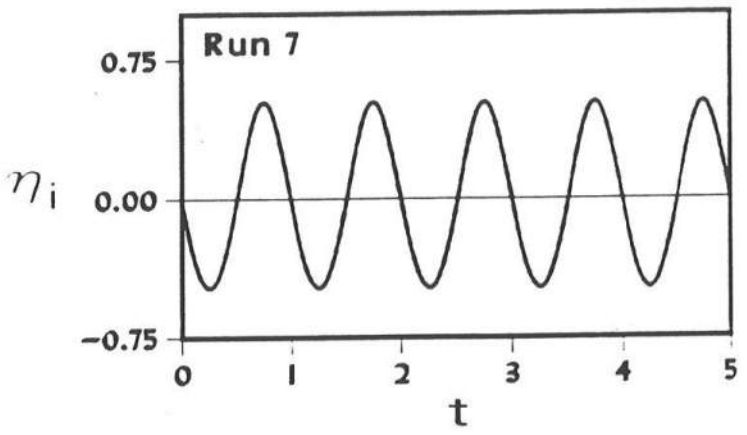
Run 7
0.75
η_i
0.00
−0.75
0
1
2
3
4
5
t

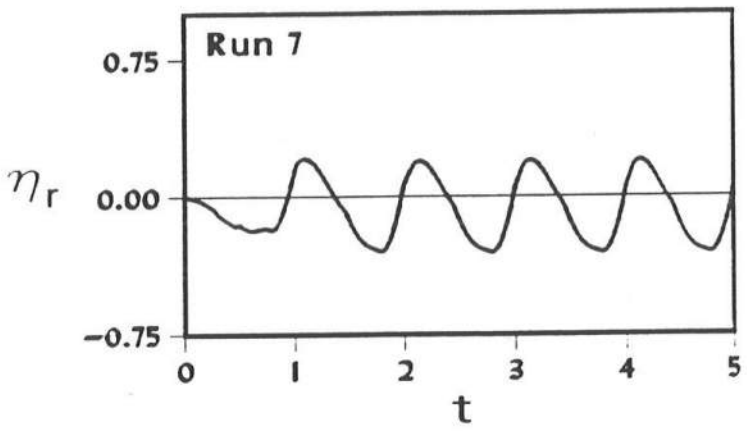
Run 7
0.75
η_r
0.00
−0.75
0
1
2
3
4
5
t

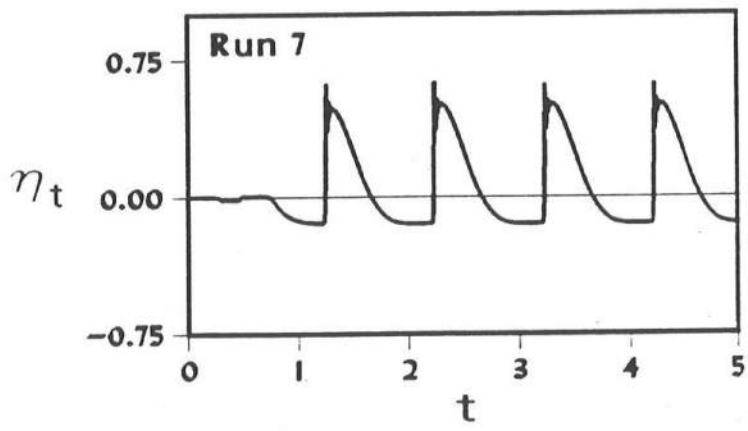
Run 7
0.75
η_t
0.00
−0.75
0
1
2
3
4
5
t

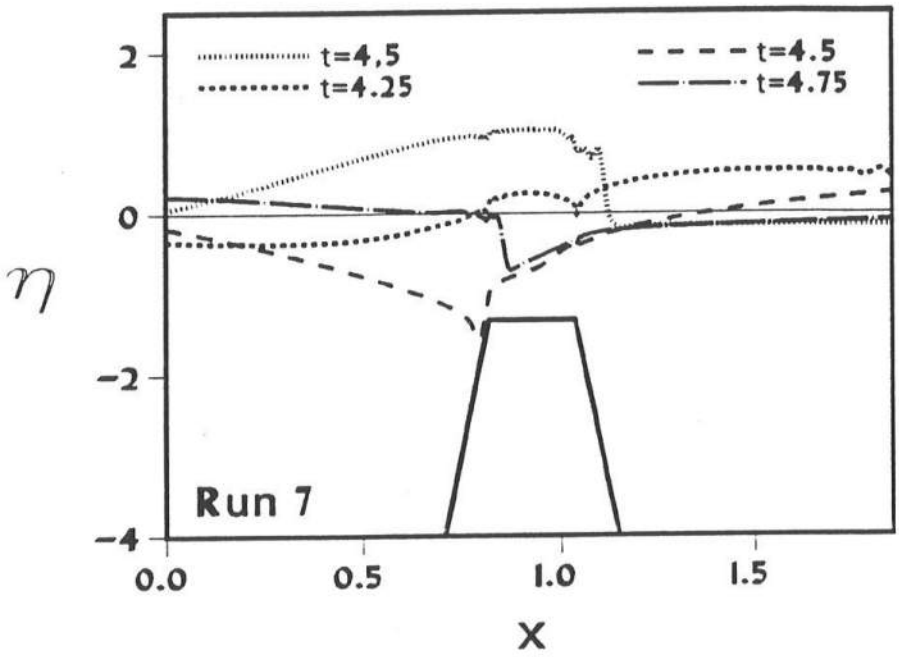
t=4,5
t=4.25
t=4.5
t=4.75
η
Run 7
2
0
−2
−4
0.0
0.5
1.0
1.5
X

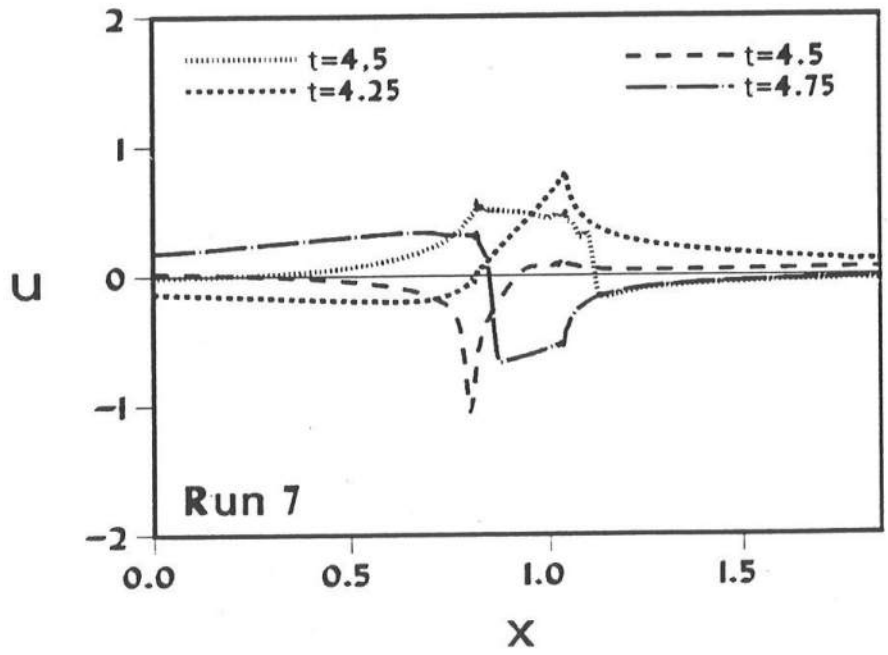
t=4,5
t=4.25
t=4.5
t=4.75
u
Run 7
2
1
0
−1
−2
0.0
0.5
1.0
1.5
X

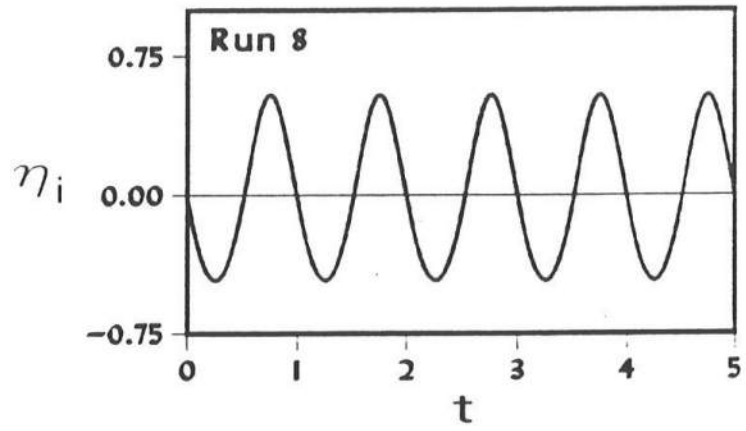
Run 8
0.75
0.00
−0.75
η_i
0
1
2
3
4
5
t

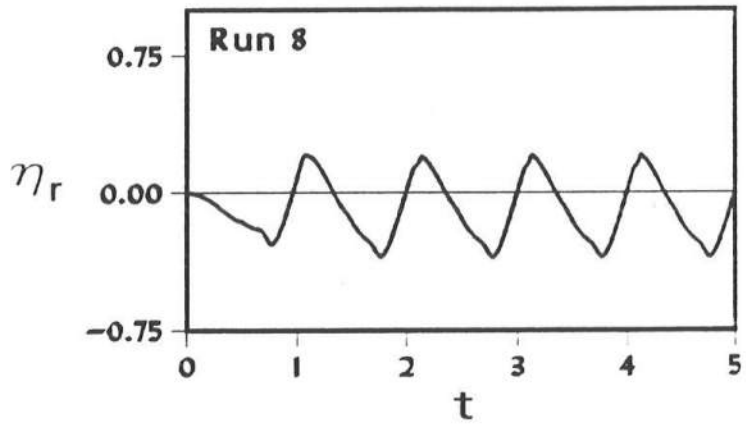
Run 8
0.75
0.00
−0.75
η_r
0
1
2
3
4
5
t

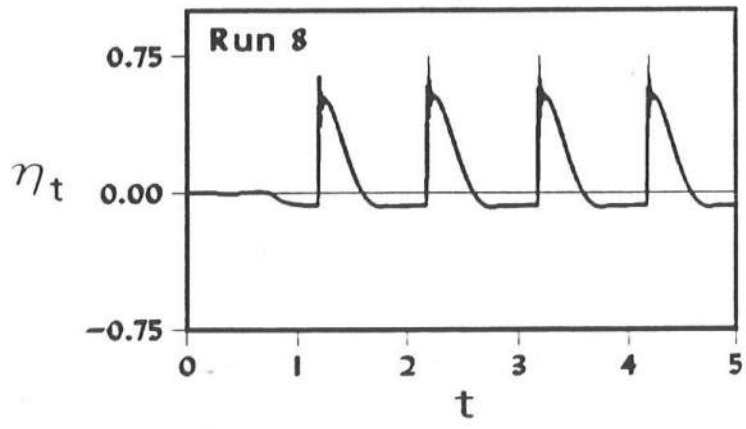
Run 8
0.75
0.00
−0.75
η_t
0
1
2
3
4
5
t

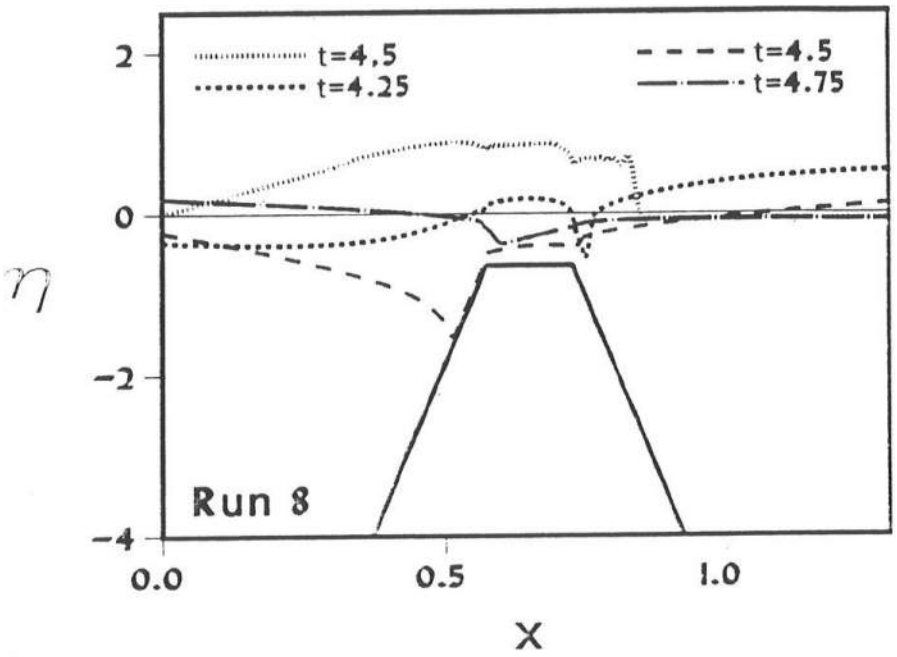
t=4,5
t=4.25
t=4.5
t=4.75
2
0
−2
−4
η
Run 8
0.0
0.5
1.0
X

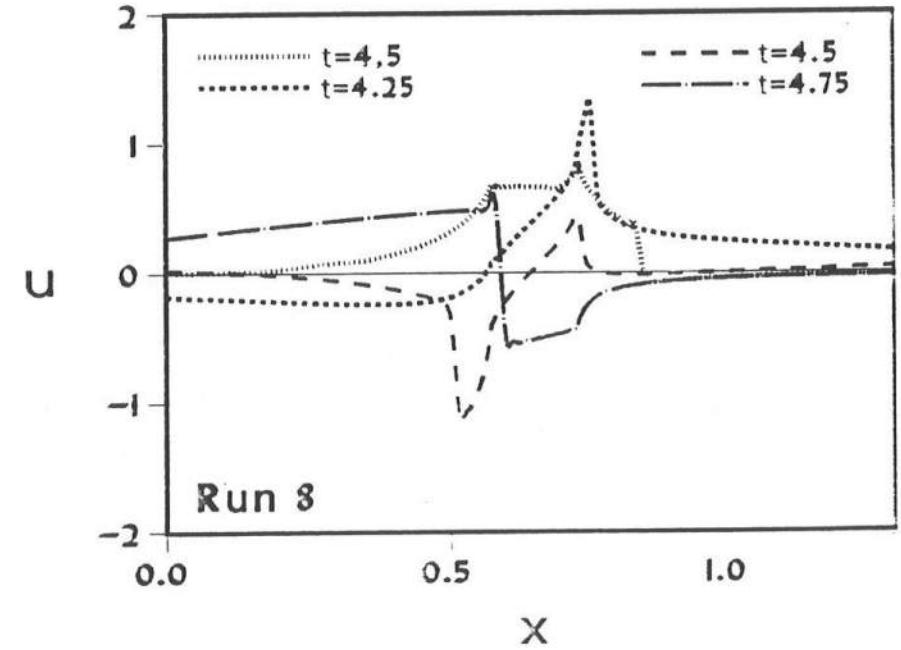
t=4,5
t=4.25
t=4.5
t=4.75
2
1
0
−1
−2
u
Run 8
0.0
0.5
1.0
X

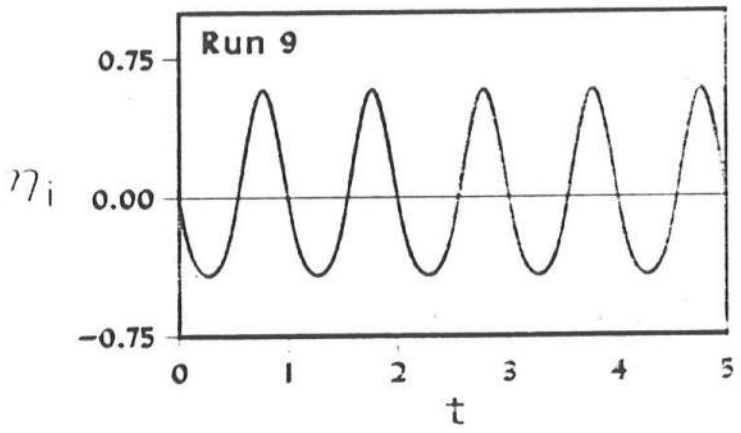
Run 9
0.75
0.00
−0.75
η_i
0
1
2
3
4
5
t

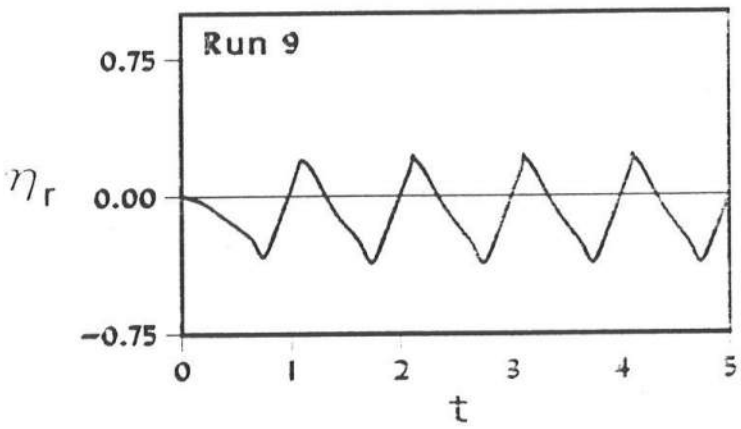
Run 9
0.75
0.00
−0.75
η_r
0
1
2
3
4
5
t

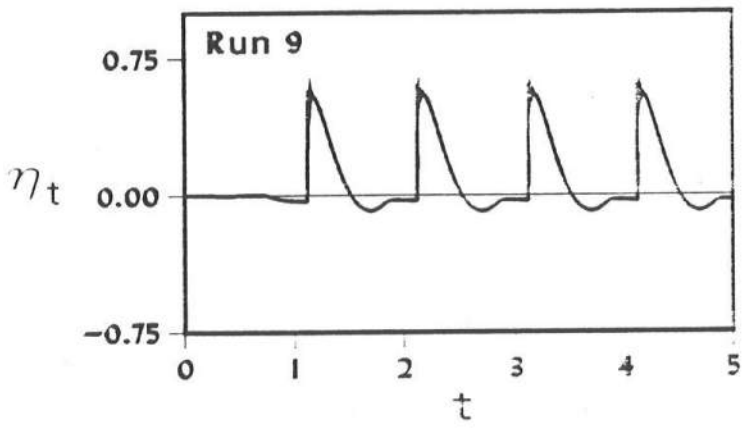
Run 9
0.75
0.00
−0.75
η_t
0
1
2
3
4
5
t

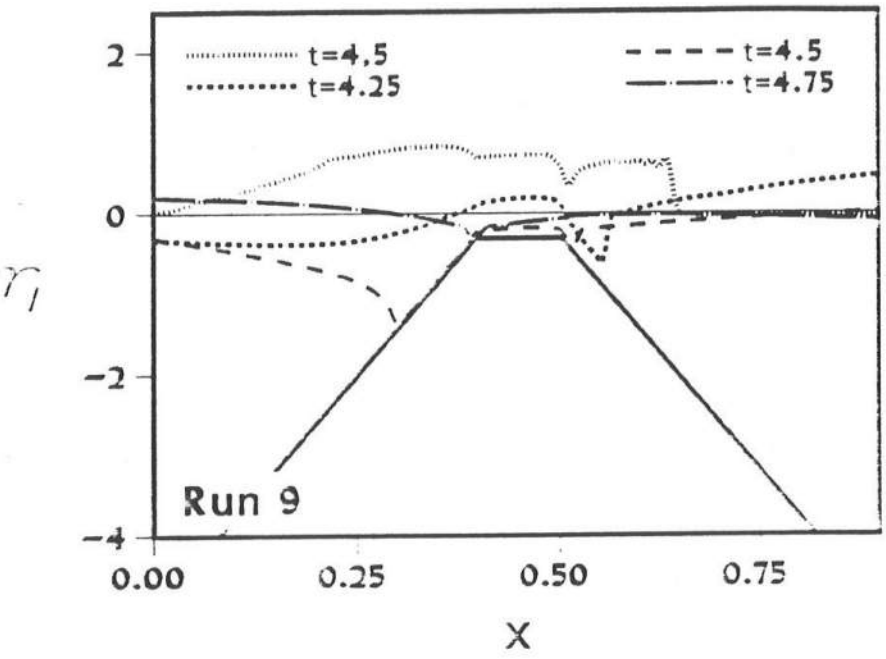
t=4.5
t=4.25
t=4.5
t=4.75
2
0
-2
-4
η
Run 9
0.00
0.25
0.50
0.75
X

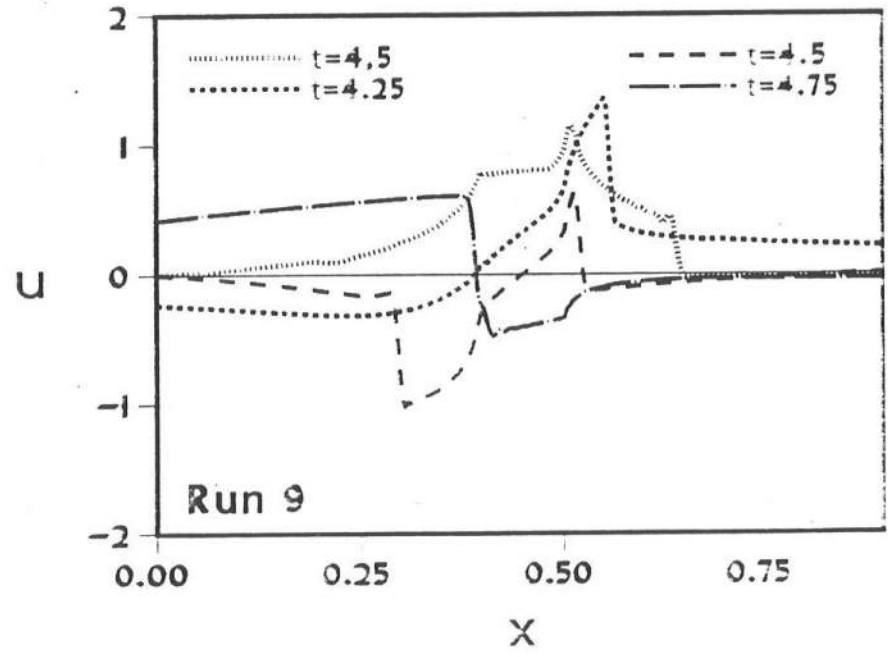
t=4.5
t=4.25
t=4.5
t=4.75
2
1
0
-1
-2
u
Run 9
0.00
0.25
0.50
0.75
X

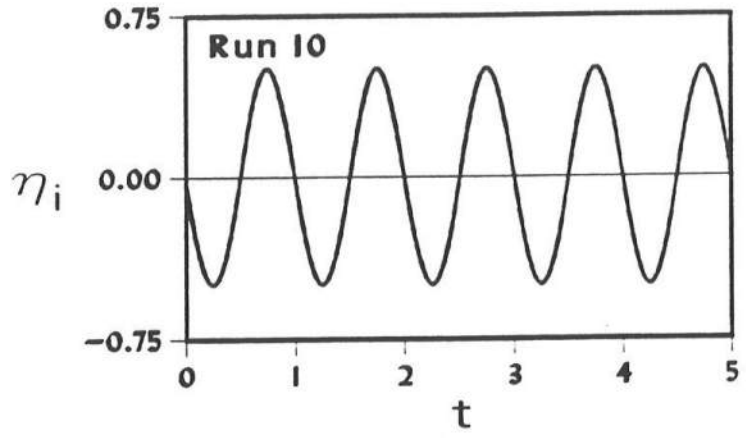
Run 10
0.75
0.00
−0.75
η_i
0
1
2
3
4
5
t

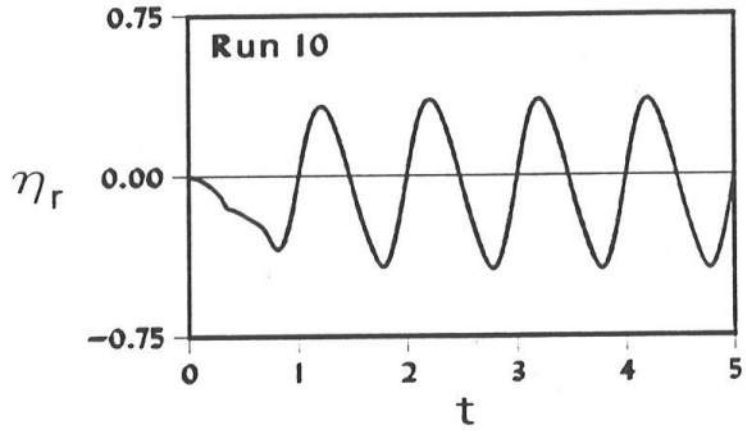
Run 10
0.75
0.00
−0.75
η_r
0
1
2
3
4
5
t

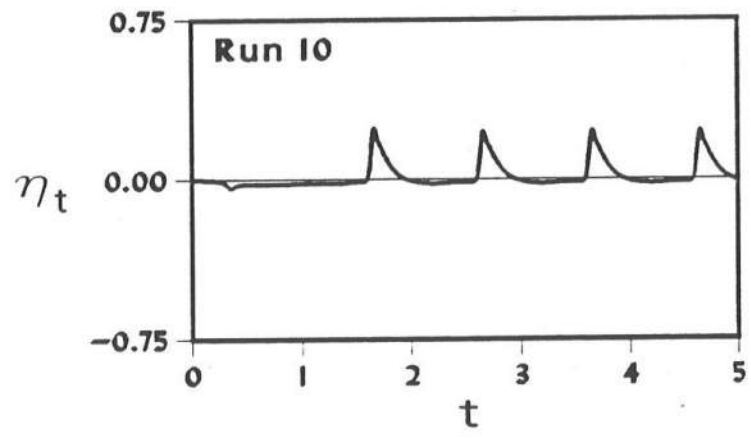
Run 10
0.75
0.00
−0.75
η_t
0
1
2
3
4
5
t

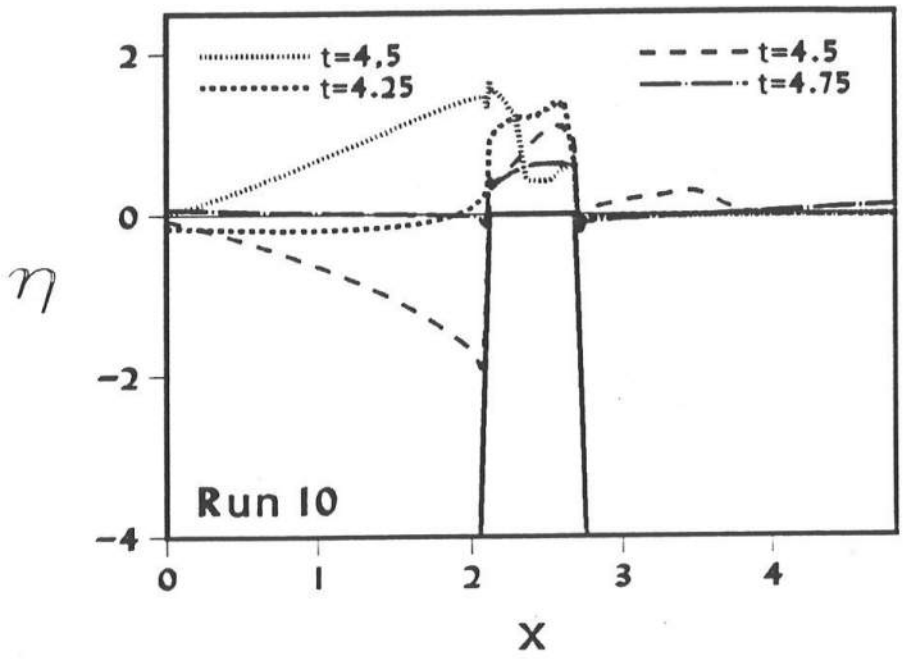
t=4,5
t=4.25
t=4.5
t=4.75
Run 10
η
X

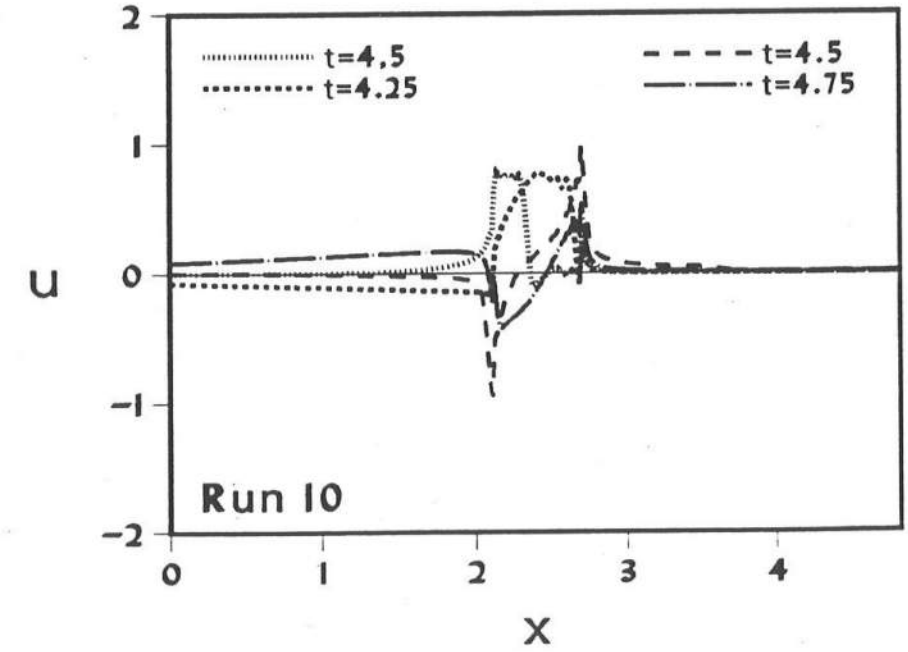
t=4,5
t=4.25
t=4.5
t=4.75
Run 10
u
X

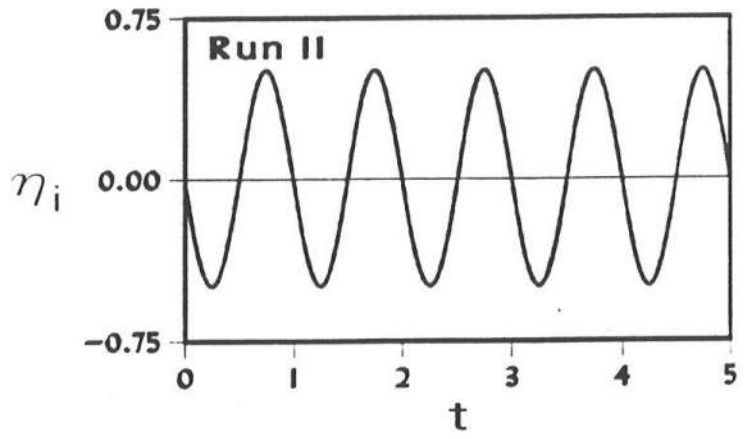
Run II
η_i
0.75
0.00
−0.75
0
1
2
3
4
5
t

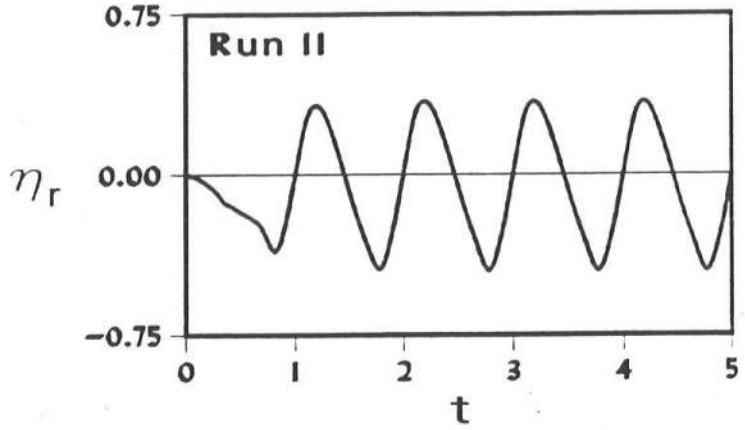
Run II
η_r
0.75
0.00
−0.75
0
1
2
3
4
5
t

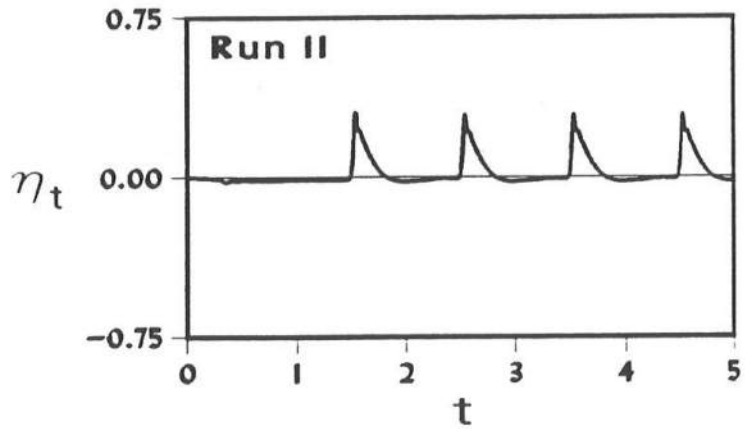
Run II
η_t
0.75
0.00
−0.75
0
1
2
3
4
5
t

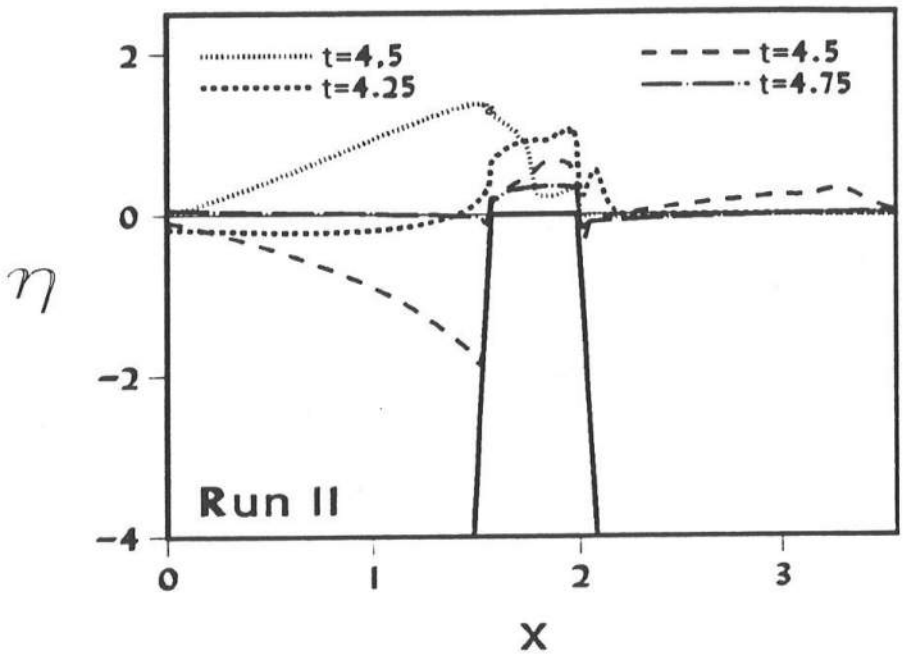
t=4,5
t=4.25
t=4.5
t=4.75
Run II
η
X

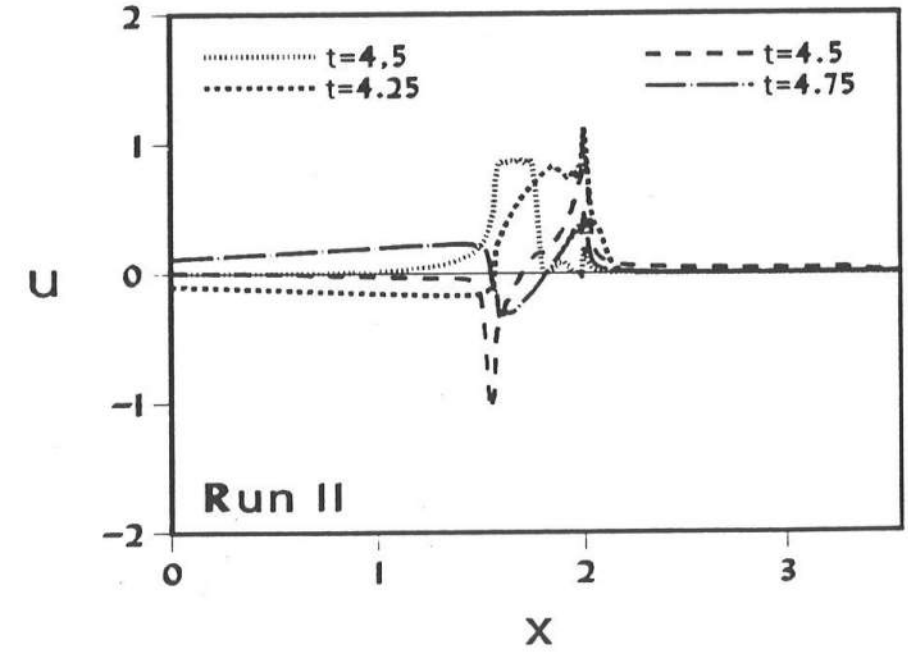
t=4,5
t=4.25
t=4.5
t=4.75
Run II
u
X

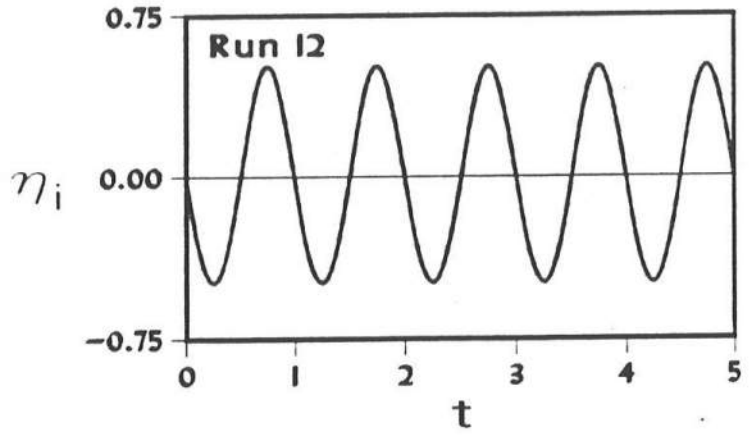
Run 12
0.75
0.00
−0.75
η_i
0
1
2
3
4
5
t

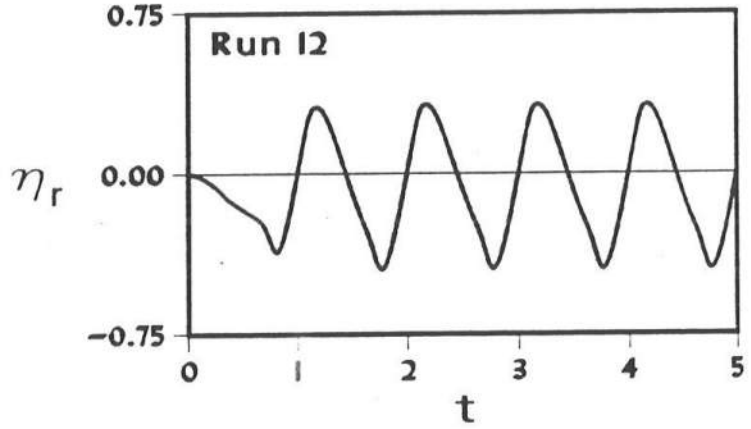
Run 12
0.75
0.00
−0.75
η_r
0
1
2
3
4
5
t

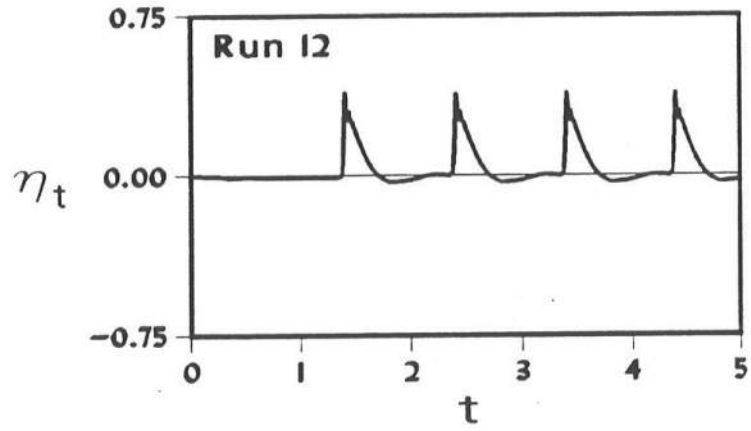
Run 12
0.75
0.00
−0.75
η_t
0
1
2
3
4
5
t

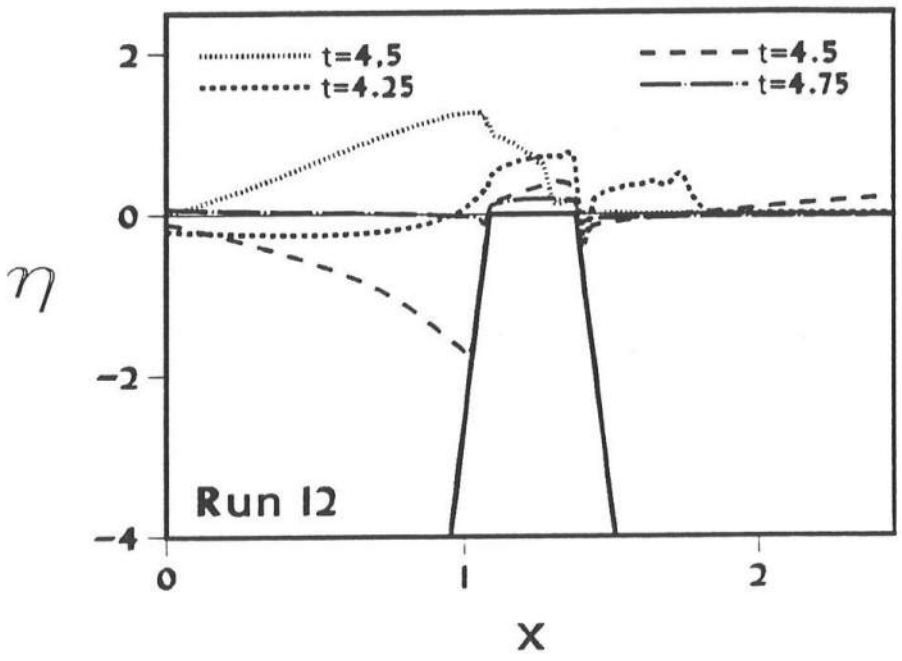
t=4.5
t=4.25
t=4.5
t=4.75
Run 12
η
2
0
-2
-4
0
1
2
X

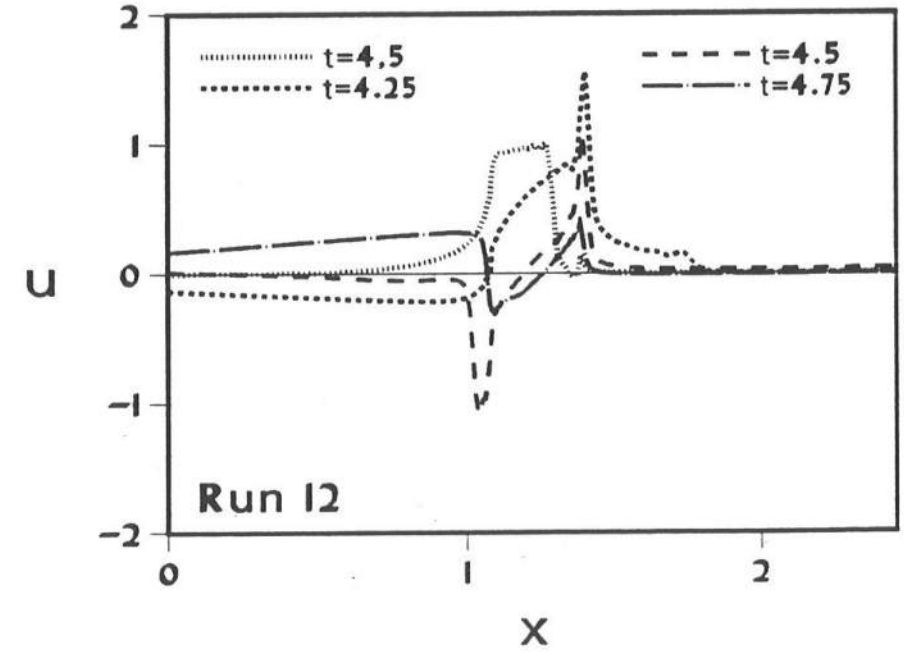
t=4.5
t=4.25
t=4.5
t=4.75
Run 12
u
2
1
0
-1
-2
0
1
2
X

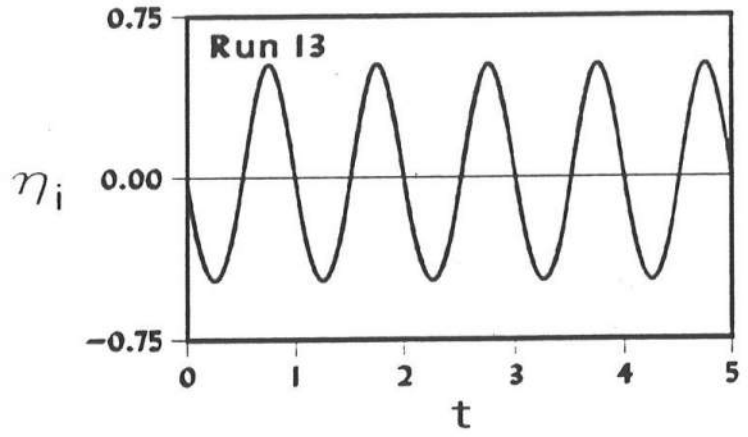
Run 13
0.75
0.00
−0.75
η_i
0
1
2
3
4
5
t

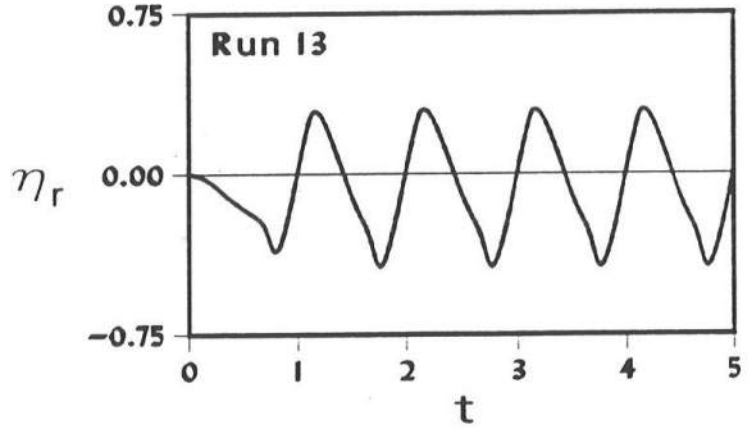
Run 13
0.75
0.00
−0.75
η_r
0
1
2
3
4
5
t

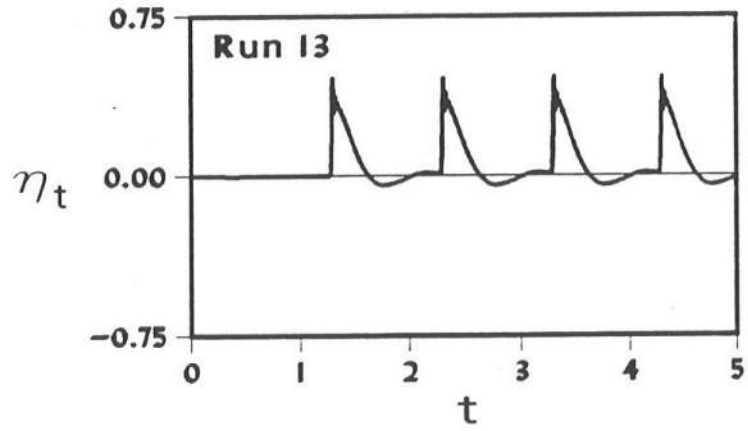
Run 13
0.75
0.00
−0.75
η_t
0
1
2
3
4
5
t

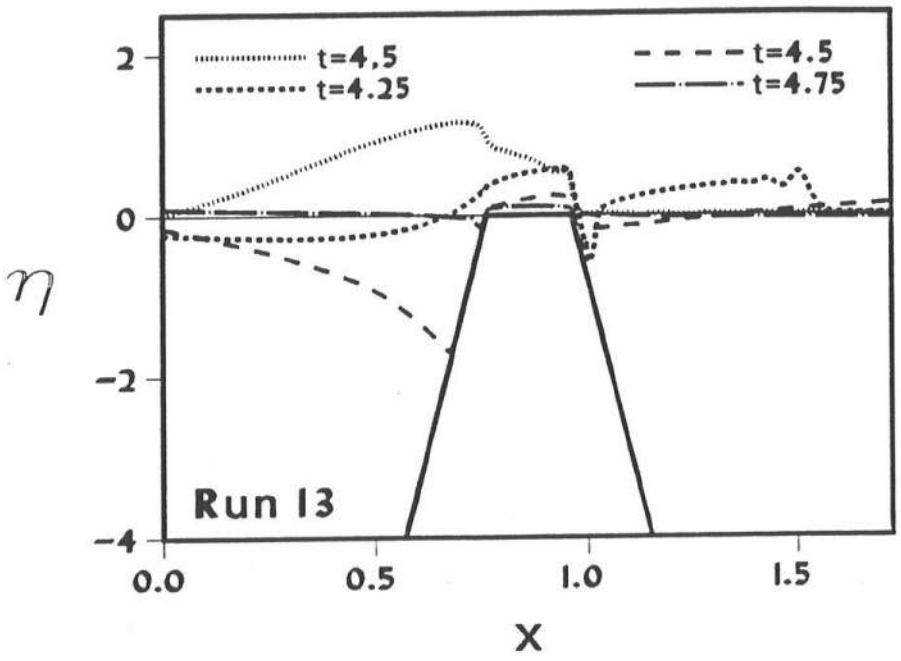
t=4.5
t=4.25
t=4.5
t=4.75
Run 13
η
2
0
-2
-4
0.0
0.5
1.0
1.5
X

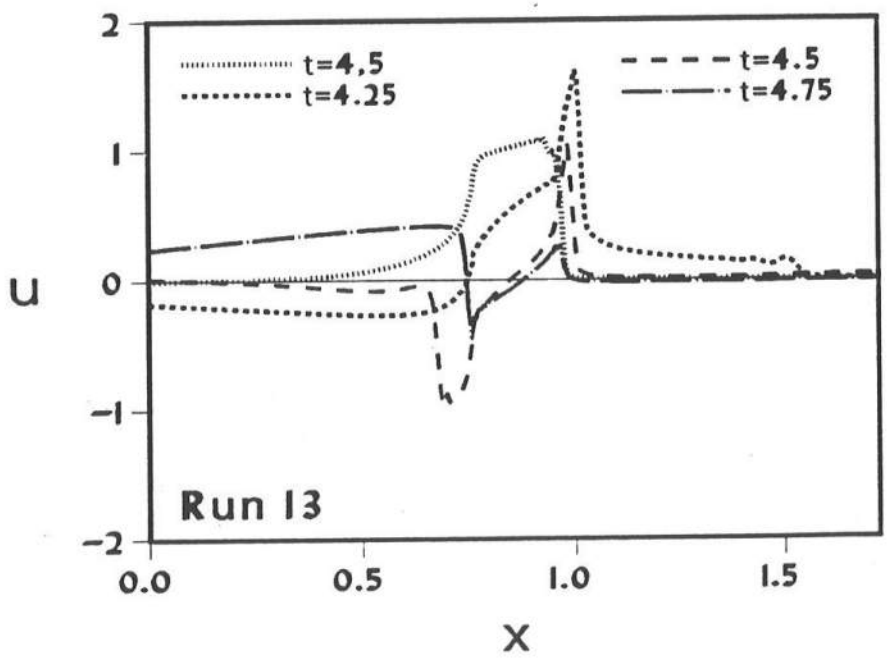
t=4.5
t=4.25
t=4.5
t=4.75
Run 13
u
2
1
0
-1
-2
0.0
0.5
1.0
1.5
X

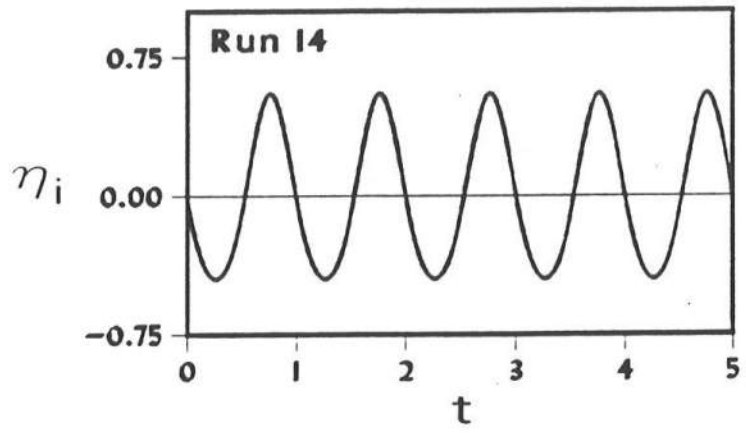
Run 14
0.75
0.00
−0.75
η_i
0
1
2
3
4
5
t

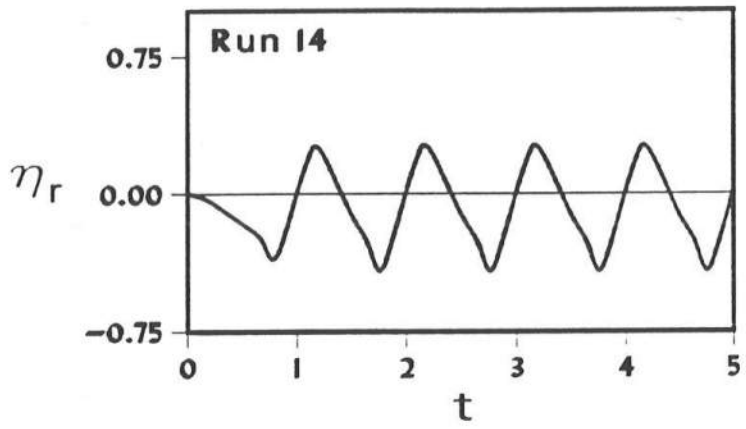
Run 14
0.75
0.00
−0.75
η_r
0
1
2
3
4
5
t

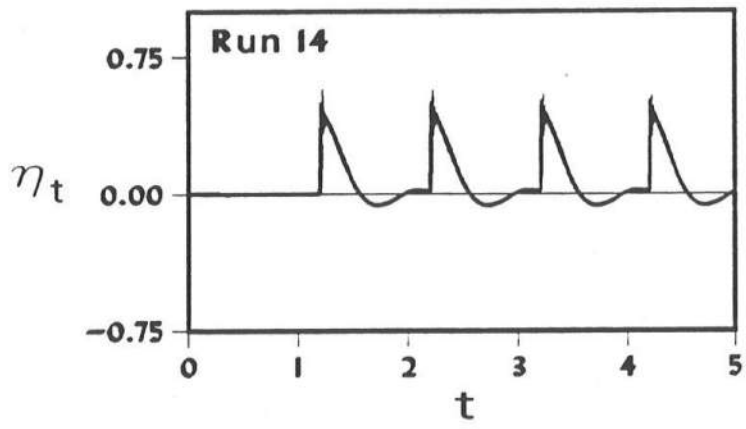
Run 14
0.75
0.00
−0.75
η_t
0
1
2
3
4
5
t

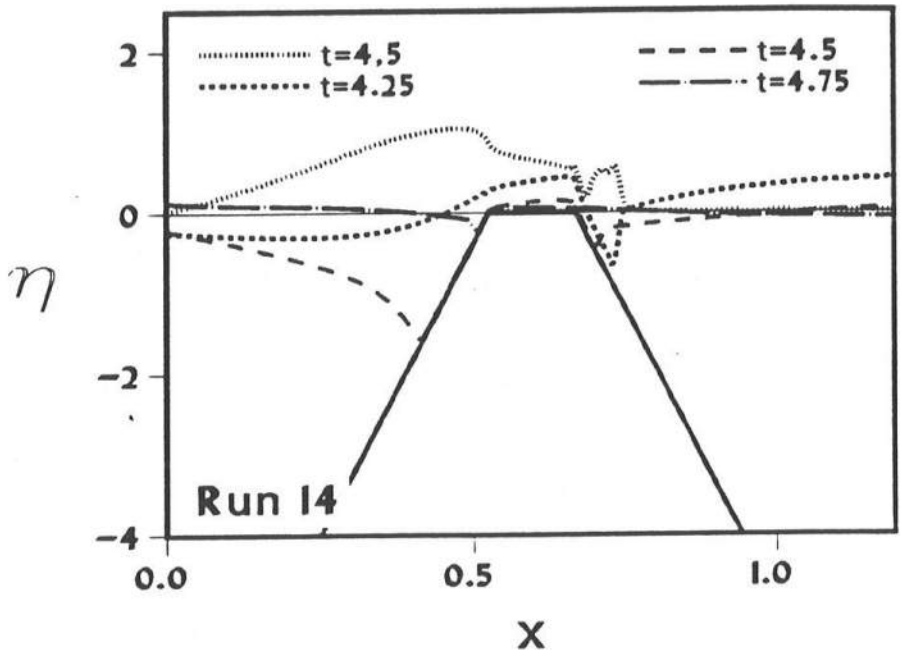
t=4.5
t=4.25
t=4.5
t=4.75
Run 14
η
2
0
-2
-4
0.0
0.5
1.0
X

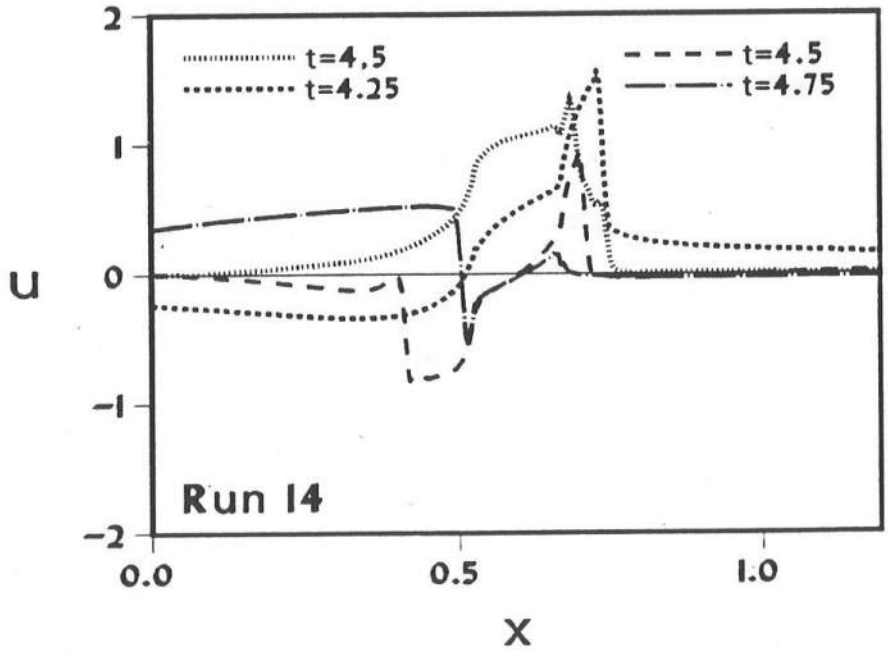
t=4.5
t=4.25
t=4.5
t=4.75
Run 14
u
2
1
0
-1
-2
0.0
0.5
1.0
X